POLITECNICO DI TORINO

Corso di Laurea Magistrale in Ingegneria Biomedica

Tesi di Laurea Magistrale

Ballistocardiographic heart and breathing rates detection

Relatore:
Prof.ssa Gabriella Olmo

Candidato:
Emanuela Stirparo

ANNO ACCADEMICO 2018-2019

Acknowledgements

A conclusione di questo lavoro di tesi vorrei ringraziare tutte le persone che mi hanno sostenuta ed accompagnata lungo questo percorso.

Ringrazio la Professoressa Gabriella Olmo per avermi dato la possibilità di svolgere la tesi nell'azienda STMicroelectronics e per la disponibilità mostratami.

Ringrazio l'intero team: Luigi, Stefano e in particolare Marco, Valeria ed Alessandro per avermi aiutato in questo percorso con suggerimenti e consigli. Grazie per essere sempre stati gentili e disponibili, sia in campo professionale che umano. Un ringraziamento lo devo anche a Giorgio, per avermi fornito tutte le informazioni e i dettagli tecnici in merito al sensore utilizzato. Vorrei ringraziare anche tutti i ragazzi che hanno condiviso con me questa esperienza ed hanno contribuito ad alleggerire le giornate lavorative in azienda.

Ringrazio i miei amici e compagni di università: Ilaria e Maria, le amiche sulle quali posso sempre contare nonostante la distanza; Rocco, compagno di viaggio, per i consigli e per aver condiviso con me gioie così come l'ansia e le paure per gli esami; Valentina e Beatrice perché ci sono e ci sono sempre state; Rosy, compagna di studi ma anche di svago; Sara, collega diligente e sempre con una parola di supporto, grazie soprattuto per tutte le dritte di questo ultimo periodo.

Il più grande ringraziamento va ai miei genitori, il mio punto di riferimento, il mio sostegno di questi anni. Grazie mamma e papà per avermi sostenuta sempre, dandomi la possibilità di raggiungere questo traguardo.

Grazie anche a mia sorella, Mariella, per avermi supportata e "sopportata" in questo anno. La ringrazio soprattutto per l'impegno mostrato nel reclutamento di soggetti, necessari per l'acquisizione del segnale BCG, ed essersi prestata lei stessa in prima persona molto pazientemente.

Un ultimo ringraziamento va ai miei nonni e zii per aver creduto sempre in me.

Summary

Cardiorespiratory diseases are becoming one of the major causes of death; for this reason, there is an increasing interest in the health surveillance. Monitoring vital signs, such as heart and respiratory rates, is a valuable tool to detect abnormalities in an individual's health. Since most conventional techniques are invasive or require the presence of medical staff, the need for continuous remote monitoring is increasing, even to reduce hospital costs. This thesis presents a contactless method to detect ballistocardiographic heart and breathing rates, in the home environment, of a subject lying comfortably on his/her bed. These vital signs could subsequently be used for sleep analysis. The main goals of this study are setting of measurement system, in order to acquire good quality ballistocardiographic (BCG) signals, heart and respiratory rates detection and their validation. To record the signal, an accelerometer has been properly placed on the bed; subsequently, the heart and breathing rates are extracted with a time-domain algorithm, which is one of the classes of methods used in literature for processing the BCG signal. Time-domain algorithms are highly affected by motion artifacts but, compared with the frequency-domain algorithms, they provide reliable information about the heart rate variability. Moreover, they have a lower computation cost than time-frequency analysis. The proposed algorithm is divided in two parts: the pre-processing step, with which the out-of-band components are removed, and the heart and breathing rates detection. To evaluate the achieved results, heart rate and breathing rate values are compared with the values obtained from the BodyGateWay, a biomedical device developed by STMicroelectronics used for remote monitoring. The thesis is organized as follows. The first chapter provides an overview of cardiorespiratory monitoring techniques, with respective advantages and disadvantages; the second chapter covers the details of BCG signal (a mechanical measure of repetitive movements of the human body due to the acceleration of blood in large vessels during each cardiac cycle); the third chapter illustrates the sensors and techniques used in literature to acquire and process the BCG signal; the fourth chapter describes the proposed algorithm to extract heart and respiratory rates; the fifth chapter deals with the tested sensors (i.e. 2 accelerometers developed by the STMicroelectonics), the measurement setup and the obtained results. Finally, future developments of this application are discussed.

List of acronyms

ACG	Apex cardiogram
ANN	Artificial Neural Network
BCG	Ballistocardiogram
BGW	BodyGateWay
BRV	Ballistocardiographic Respiratory Variation
CA	Cluster Approach
cECG	Capacitive Electrocardiogram
CEEMDAN	Complete Ensemble Empirical Mode Decomposition with Adaptive Noise
CWT	Continuous Wavelet Transform
DB-BCG	Direct Body Ballistocardiogram
DWT	Discrete Wavelet Transform
ECG	Electrocardiogram
EEMD	Ensemble Empirical Mode Decomposition
EMD	Empirical Mode Decomposition
FBGS	Fiber Bragg Grating Sensors
FFT	Fast Fourier Transform
FT	Fourier Transform
HF-BCG	High Frequency Ballistocardiogram
HR	Heart Rate

HRV	Heart Rate Variability
HT	Hilbert Transform
ICG	Impedance Cardiogram
ICT	Information and Communication Technologies
IMF	Intrinsic Mode Function
LF-BCG	Low Frequency Ballistocardiogram
MA	Moving Average
MAE	Mean Absolute Error
MEMS	Micro-Electro-Mechanical-System
MFOS	Micro-bend Fiber-Optic Sensors
MLP	Multilayer Perceptron
NADA	Noise-Assisted Data Analysis
PCA	Principal Component Analysis
PCG	Phonocardiogram
PPG	Photoplethysmography
PPGI	Photoplethysmographic Imaging
PSD	Power Spectral Density
PSG	Polysomnography
PPV	Positive Predictive Value
RCL	Respiration Cycle Length
RMSE	Root Mean Square Error
RR	Respiratory Rate
SCG	Seismocardiogram
STFT	Short-Time Fourier Transform
TFD	Time-Frequency Distribution

UF-BCG Ultra-low Frequency Ballistocardiogram

WHO World Health Organization

WT Wavelet Transform

Contents

Chapter 1

Introduction

Cardiorespiratory diseases affect a large part of the population over the age of 40 and are becoming one of the major causes of death. Moreover, healthcare cost will increase due to the demographic changes. Consequently, it is important to emphasize early detection and timely diagnosis both for patients'survival and cost reduction [1, 2]. Daily monitoring of vital signs, such as heart rate and respiratory rates, is useful for detecting and preventing cardiorespiratory dysfunctions; in particular, nocturnal monitoring allows the assessment of sleep quality, which is closely related to the proper functioning of the immune system and to some psychosomatic states. Numerous non-invasive techniques have been developed for monitoring physiological parameters in order to overcome limits of conventional clinical methods. The main disadvantages of current medical techniques include poor compliance, restriction of patient's movement by cables and sensors and the need for direct skin contact. The overcoming of these limits could be achieved with the possibility of monitoring the physiological parameters in a completely non-invasive way, if possible contactless but guaranteeing the reliability of the measurements. Home monitoring will play a significative role in future healthcare systems because it offers greater comfort, reduces the chance of rehospitalization, provides early diagnosis and decreases mortality rate [3]. In this thesis a contactless heart and breathing rates monitoring is presented using a mechanical signal, the ballistocardiogram.

1.1 Current cardiorespiratory and sleep monitoring techniques

Monitoring and diagnostic systems allow to measure physiological parameters, such as respiratory and cardiac activity, blood pressure and oxygen saturation. Each of these methods is based on a particular physiological effect which can be measured in a non-invasive and unobtrusive way. Despite measurement modalities yield good results in clin-

ical practice, they may be uncomfortable and, in most cases, they need the presence of medical staff. In contrast, unobtrusive tests are easy to perform and are a valuable tool for long-term monitoring of some cardiac conditions. Regarding sleep monitoring, the gold-standard is the polysomnography (PSG); this is a physical exam performed with different types of electrodes and sensors for monitoring various body functions during sleep. Despite it is a complete diagnostic test (determining sleep stages, sleep quality and sleep disorders), the PSG is rather uncomfortable, expensive and intrusive; furthermore, the instrumentation could alter the subject sleep and it is not suitable for continuous long-term measurements [4]; hence, the limitations of this medical procedure are its invasiveness, complexity and limitation to a hospital setting. As for the cardiorespiratory monitoring, current techniques are based on bioelectrical, mechanical or thermal effects [1].

1.1.1 Bioelectrical effect-based techniques

During the cardiac cycle, the electrical excitation of the cardiac muscle cells generates a voltage signal on the body surface that can be measured with the electrocardiogram (ECG), or capacitive electrocardiogram (cECG), which is considered the gold-standard for cardiac monitoring. Although the ECG is a very reliable test, it requires an accurate application of several electrodes on the chest (in order to measure any electrical activity of the heart, at least two electrodes are required) [5] and, for this reason, it may be uncomfortable for the patient.

1.1.2 Mechanical effect-based techniques

The exchange of air inside the lungs and the pumping of blood through the vascular system result in a deformation of the organ and fluid displacement. For example, blood movements cause microscopic rhythmic expansion and contraction of the arteries which result in changes of the optical skin properties. Methods based on this effect (superficial perfusion) are photoplethysmography (PPG) and photoplethysmographic imaging (PPGI). The PPG is a superficial optical measurement and, being minimally invasive, it is of great interest; besides, it can be acquired in various parts of the body. The volume of blood inside the blood vessels changing accordingly to heart pumping and it causes a variation in vessels dimensions. If a blood vessel (or an amount of blood vessels) is lighted up, the light absorption will be proportionally to volume blood itself; therefore, heart and breathing rates can then be obtained from PPG signal. Additionally, since oxygenated hemoglobin has a different absorption spectrum than deoxygenated hemoglobin, it is possible to determine the oxygen saturation. Another consequence of changes in lungs size during the respiratory cycle and deformation of the heart during the cardiac cycle is body surface displacement. The sensor-based technologies which rely on these effects are ballistocar-

diographic, seismocardiographic, radar-based, laser-based and video-based motion analysis methods [1]. As their names imply, ballistocardiogram and seismocardiogram (SCG) refer only to the cardiac component but they can also be used to analyze the respiratory activity because they usually contain a superimposed respiratory component. The BCG signal, in particular, is generated by body movements due to ejection of blood into the arteries and can be recorded using wearable or fixed sensors. The origin of this signal is not fully known yet, but it is accepted that the "IJK" complex corresponds to the ventricular systole. HR, HRV, RR and blood pressure can be obtained from the BCG. Additionally, this signal is closely bound to the fluid-dynamic forces of the blood, thus hemodynamic parameters such as cardiac output can also be estimated. However, a drawback of the BCG signal is its dependency on the measurement method and on subject's characteristics such as age or health conditions. For these reasons, ballistocardiography is more appropriate for long-term monitoring than for comparative assessments among subjects in a population. With the SCG, instead, the movement of the chest wall is monitored following breathing or heartbeat attaching a high-sensitivity accelerometer to the subject's thorax [6]. Due to the placement of this sensor, the SCG also includes high frequency content correlated to the closure of the heart valves. Finally, it is known that not all effects caused by cardiorespiratory activity can be detected with measurement on the body surface [1]. For example, the local changes in the dielectric properties of the thorax during the cardiac and respiratory cycles can be measured using high frequency electromagnetic fields. The method based on this effect is the impedance cardiogram (ICG), obtained by injecting a current into the body and subsequently reading the voltage drop through the electrodes placed on the body. This measure provides information on respiratory rhythm and cardiac output; however, being based on the use of electrodes, ICG has the same limitations of ECG. Figure 1.1 shows the ECG, SCG, BCG and ICG signals.

1.1.3 Thermal effects-based techniques

Thermography, based on far-infrared or mid-infrared image acquisition, is a promising technique to assess vital parameters, such as RR and HR, that can be detected from the signals produced by the air flowing through the nostrils and the superficial blood flow, which imply a change in temperature [1]. Both these signals have a mechanical nature and are related to surface perfusion. Detecting the radiation naturally emitted by human skin through a thermal imaging camera, thermography is a contactless technology; it is a monitoring approach that allows remote reading of the temperature distribution of the body area of interest. The most important advantage of thermal imaging is that it does not need an external radiation source [7]. However, it is an expensive technique and it cannot be performed at home.

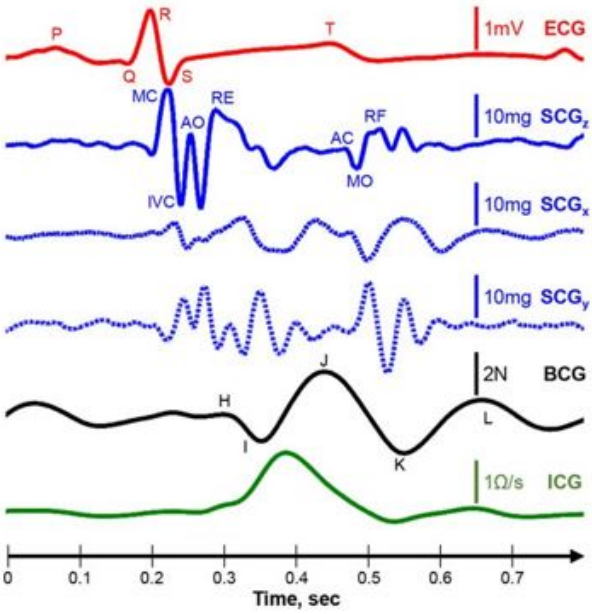

Figure 1.1: Simultaneously acquired ECG, SCG, BCG and ICG signals [8]

1.2 Motivation

Vital signs, such as cardiac and respiratory parameters, are good indicators of a person's general health and life expectancy. Typically, their measurements require the presence of a doctor and invasive means. In order to address patient convenience and quickly obtain the desired information, numerous methods and wearable devices (such as patches, bands, bracelets or T-shirts) have been developed for cardiorespiratory monitoring. The advantages of these instruments are their 24-hour continuous monitoring capability, real-time results and interpretation of the recorded signals. With this approach, patients can monitor their health at home. Despite the advantages of wearable devices, the patient have to wear its and, in many cases, that devices are very uncomfortable, especially during sleep phase. Home monitoring systems should be able to provide significant and reliable information about patient's health status without be invasive and demanding under point of view of presence and maintenance [3]. For these reasons, telemedicine applications are constantly developing to make signal acquisition mechanisms increasingly reliable and less invasive. Recent studies have shown that home telehealth methods can lead to a considerable reduction of hospital admissions and numbers of bed days of care [9].

1.3 Telemedicine

The prefix "tele" is a Greek word meaning "at a distance", "far" or "remote", hence the term telemedicine literally means "medicine delivered at a distance" [10]. It is an open and constantly evolving science because it includes new advancements in technology and adapts to the changing health needs of society. Figure 1.2 shows the telemedicine architecture.

> "Telemedicine involves the use of modern information technology, especially two-way interactive audio/video communications, computers, and telemetry, to deliver health services to remote patients and to facilitate information exchange between primary care physicians and specialists at some distances from each other" (Bashshur, *et al*, 1997).

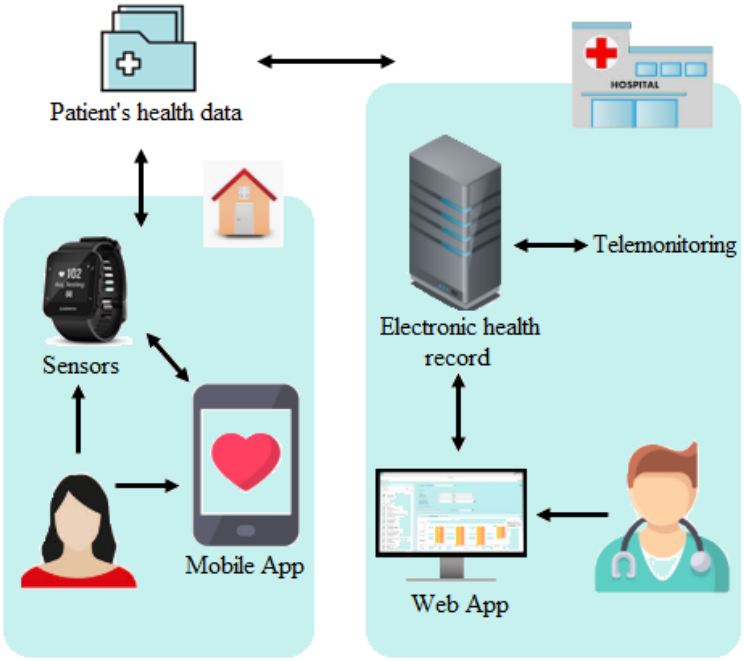

Figure 1.2: Telemedicine architecture

The term "telemedicine" is different from "telehealth" and "telecare". The three terms are included in the broad concept of "eHealth" (Figure 1.3) but differ in the way information and communication technologies (ICT) are used to provide healthcare services. There is not a consensual definition for eHealth but according to World Health Organization (WHO), it refers to the use of ICT to recover, store or share health data for prevention, diagnosis, treatment, monitoring, educational and administrative purposes. Telehealth is a subset of eHealth and includes a vast range of services and technologies

to provide patient care remotely; its primary goal is to improve the healthcare system; it has a broader meaning, in fact telehealth refers not only to clinical services but also to administrative and educational services provided by health professionals in general, such as nurses, pharmacists, and others. Telemedicine is a subsection of telehealth that involves ICT and software to provide clinical services to patients at home but also to transfer medical information for therapy and diagnosis. It is only related to clinical health care services. Examples of assistances that can be provided at a distance, especially via video-conferencing or interactive audio communication, are medication management and specialist consultation. Lastly, telecare describes the application of telemedicine to provide care services to patients in their own homes; it refers to the continuous and remote monitoring of users through sensors [11].

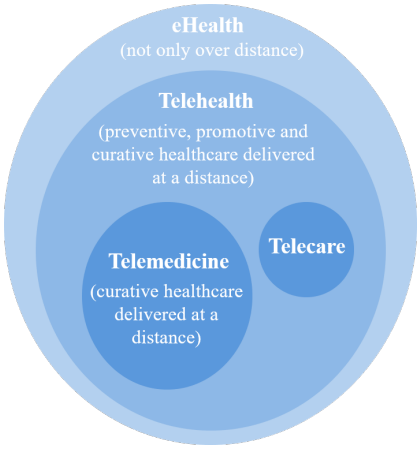

Figure 1.3: Relations among eHealth, Telehealth, Telecare and Telemedicine

Telemedicine involves several services that can be used in various application areas (dermatology, radiology, pathology, psychiatry, ophthalmology, cardiology) and performed in two different ways: store-and-forward (or asynchronous) methods and real-time (or synchronous) methods:

- **Store-and-forward (or asynchronous) methods** include the exchange of pre-recorded healthcare data between two or more individuals at different times. It is relatively inexpensive and easy to use [11].
- **Real-time (or synchronous) methods** require the immediate transmission of healthcare data to allow real-time interaction between patient and healthcare professional or among specialists. The most commonly used forms of communication are video-conference, phone call and online chat [11].

In particular, telemedicine services are teletriage, teleconsultation, telediagnosis, telesurgery, telescreening and telemonitoring.

This thesis focuses on telemonitoring, which is performed in five steps:

1. Data acquisition through a specific sensor;
2. Data transmission from patient to physician;
3. Data integration with other information describing the state of patient;
4. Appropriate action and response in the care of patient;
5. Data storage.

Telemonitoring services are not primarily performed by physicians, in fact they are only involved when patients present signs of health impairment. It is important to note that telemedicine is not meant to replace traditional medicine but complements it with innovative technologies improving health care and ensuring the best care for citizens. Currently, in fact, there is an increasing need for continuous monitoring of vital signs to improve safety, comfort and way of living of patients.

1.4 Heart and respiratory rates detection using BCG signal

In the context of eHealth, the home monitoring sector is indicated by the abbreviation pHealth, which means personalized health. For a non-intrusive monitoring, BCG signal is advantageous because it can be recorded with sensors embedded in objects of common use such as beds, office chairs, weighing scales and wearable clothes (Figure 1.4).

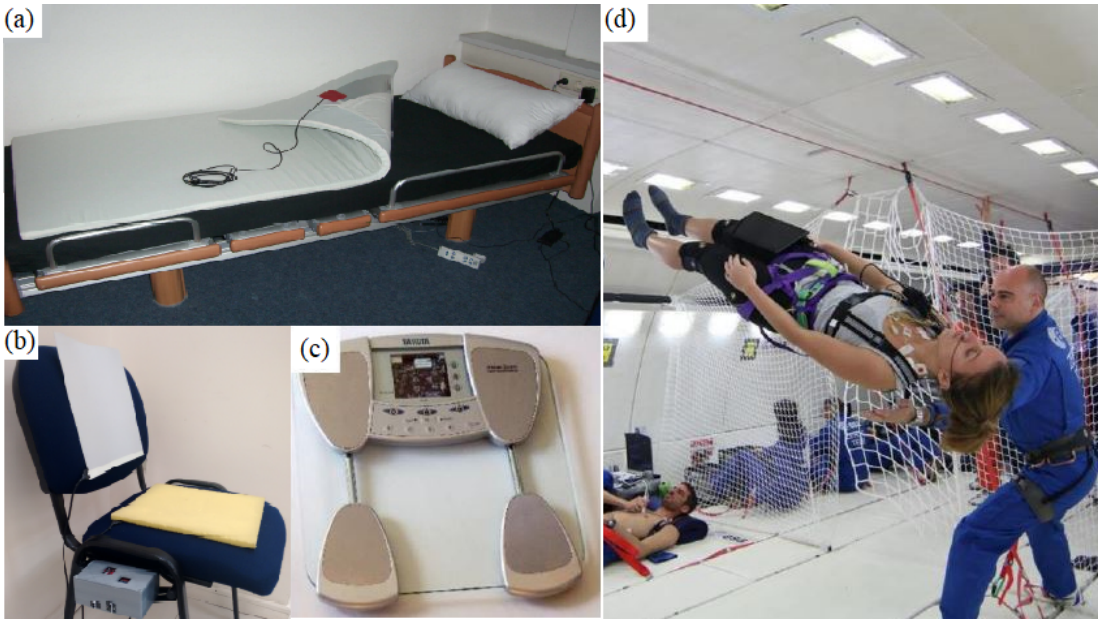

Figure 1.4: BCG acquisition hardware. (a) Emfit sensor installed on top of the bed, (b) Chair with EMFi sensors on the seat and backrest, (c) Weighing scale, (d) Wearable BCG (Pneumocard) system in micro-gravity [8, 12, 13]

While the BCG system offers the aforesaid advantages over established clinical methods, it also has inconveniences. Primarily, the signal can be highly varying due to the uncontrollable parameters of the environment in which the measurements are performed, different anthropometric characteristics and age of user. In particular, for bed-mounted sensors, the morphology of the signal is strongly influenced by the mechanical system that transmits forces and depends on the relative position and orientation of the user to the sensors [9, 14]. Robust methods are necessary to estimate vital parameters. Modeling studies are also required if there is the necessity to extract other kind of information such as cardiac output. This thesis focuses on the BCG signal because, although it has a small amplitude of about 0 - 7 milli-gravity (mg) [15] and is susceptible to noise and electrical and mechanical interference, being completely non-invasive, it is an efficient, affordable and simple solution for long-term monitoring of HR, HRV, RR and body movements. Furthermore, night heart rate can be extracted, which can subsequently be correlated with the quality and quantity of sleep and stress conditions of the patient. Another advantage of BCG signal is that it is not affected by the "white coat effect"; this term comes from white coats typically worn by doctors; it consists of an increase in blood pressure when it is measured in a medical environment. To sum up, the ballistocardiography is a convenient, low-cost, unobtrusive and easy to use solution for home e-health monitoring.

Chapter 2

Ballistocardiography

Ballistocardiography is a non-invasive method based on the measurement of the repetitive movements of the human body due to the acceleration of blood in large vessels during each cardiac cycle. In other words, it measures mass movements of the body generated by the forces of heart contraction and gives information about the overall performance of the circulatory system. Mass movements are those of the circulating blood and the heart; they can be recorded in terms of acceleration, velocity or displacement.

2.1 Brief history of ballistocardiography

The first observations of ballistocardiography date back to 1877, when Gordon made the following observation:

> "A person standing erect in a perfectly easy posture on the bed of an ordinary spring weighing-machine, and maintaining, as far as possible, perfect stillness, will be found, if the instrument is delicately adjusted, to impart a rhythmic movement to the index, synchronous with the pulse" [16].

He later continued his research by performing measurements on subjects lying in supine position. However, only in 1938 Isaac Starr and his department created a system to measure this mechanical signal in a scientific manner. They thus coined the word "ballistocardiogram" derived from the Greek words ballein (to throw), kardia (the heart), and grafein (to write) [17]. Starr's original system is known as high-frequency ballistocardiogram (HF-BCG) and it was composed of a heavy rigid platform, supported by stiff springs, upon which the subjects would lay [18]. This system was an inspiration to following researchers who made it more accurate, developing very light and freely suspended platforms (low-frequency ballistocardiogram, LF-BCG), and also new chair-based recording methods. In 1974, Van Brummelen and Josenhans had demonstrated, for example, that ultra-low frequency beds do not significantly distort the ballistocardiogram of velocity

or acceleration. However, there were two main problems that limited the clinical use of the ballistocardiography [19]:

- Physiological interpretation of the signal, which must be performed considering:
  - The distortion introduced by the mechanical system;
  - The coupling characteristics between the recording system and the body;
  - The mechanical coupling among the diverse parts of the body;
- Electronic restrictions on the available technology.

Therefore, physicians lost interest in the BCG and preferred the traditional cardiovascular monitoring methods. In the last years, the technological developments in the electronic and biomedical fields and the advancements in signal processing renewed the interest in ballistocardiography, which has become a valid non-obtrusive technique to assess cardiovascular and respiratory activity.

2.2 Physical principle of ballistocardiography

The BCG is based on Newton's laws of motion [20]. According to the second Newton's law, the force generated by the contraction of the heart causes an acceleration of the blood mass. According to the third law of motion, the BCG signal is the result of reactions forces produced when blood is expelled from the heart and circulates in the aortic arch [21].

$$F_{blood} = -F_{body}$$

At the beginning of ventricular systole, after the opening of the aortic valve, blood is pushed from the heart to the head. This, according to Newton's third law, generates an equal but opposite recoil force (H-I waves). When the aorta turns downwards, the blood is pushed towards the feet, then the acceleration is inverted (I-J waves). Subsequently, blood flows into the arteries, thus the acceleration changes sign again with the closing of the aortic valve (J-K waves). The BCG signal then varies but it dampens before the next heartbeat (K-L-M-N waves). Therefore, the ballistocardiogram is more strictly related to the heart's force than to its output.

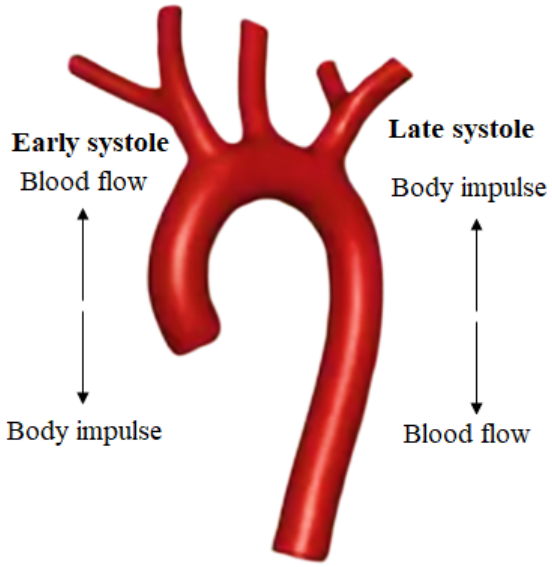

Figure 2.1: Aortic arch and force vectors during blood ejection by the left ventricle

The change of blood distribution during the cardiac cycle generates the reproducible waves of ballistocardiogram, named with capital letters (F through O). However, the major components designated by Starr are the H, I, J, K, L waves (Figure 2.2). This is the standard nomenclature of the BCG.

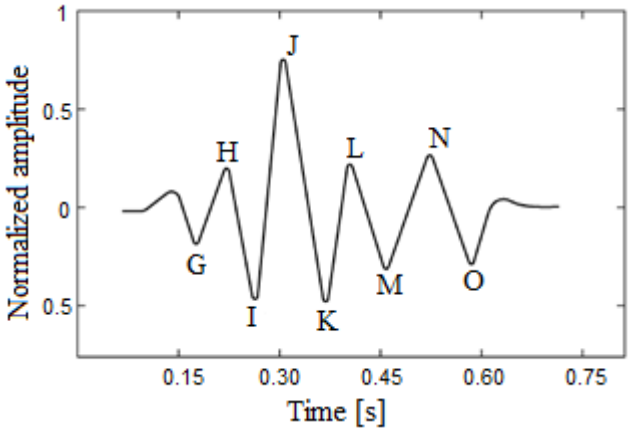

Figure 2.2: Typical BCG signal with its waves labeled

The ballistocardiographic waves are not pure forces but the resultant vectors of oppositely directed forces and are clearly associated with specific events in the cardiac cycle.

The shape and amplitude of BCG waves depend on:

- The force of myocardial contraction;
- The dynamics of the heart;
- The anatomical and physiological properties of the ventricular loads;
- The transmission characteristics of the tissues;
- The direction changes of the ejected blood mass.

The importance of the last contribution must not be undervalued because the shape of the ballistocardiogram derives from the redistribution of blood in the systemic circulation [19]. The IJK complex is of particular interest because it corresponds to the ejection phase of the heart cycle and contains the largest amplitude [22]. The vertical amplitude between the negative peak of the I-wave and positive peak of the J-wave is commonly called the I-J amplitude (Figure 2.3); it gives an index of the maximal force developed by the heart during systole because it is proportional to the blood acceleration in the ascending aorta and then in the descending and abdominal aorta [23].

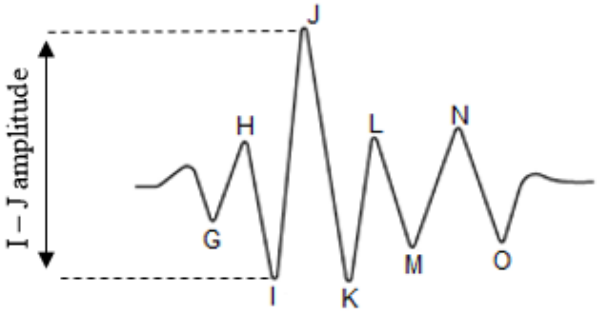

Figure 2.3: The I-J amplitude

In particular, I-wave causes the body movement in foot-ward direction because it is due to the ejection of blood in head-ward direction from the left ventricle into the aorta. J-wave, instead, causes the body movement in head-ward direction because it is due to blood movement through the descending aorta [24]. The variation of I-J amplitude is of modest degree for young subjects during ordinary respiration and it becomes more evident during deeper breathing, in normal breathing in older subjects and with heart disease.

2.3 Origin and physiological significance of the BCG waves

The ballistocardiographic waves are separated in three groups: pre-systolic, systolic and diastolic.

2.3.1 Pre-systolic group

- **F wave**. This wave is a positive deflection originated by atrial contraction. It is rarely seen but if the heart rate is slow, F wave occurs mostly. It appears simultaneously with the auricular sound, between the electrocardiographic P and Q waves [2, 21];

- **G wave**. This wave is a small foot-ward wave associated with atrial systole. G wave follows the P wave and precedes the QRS complex of the ECG signal. It is frequently seen, especially in bradycardic subjects or with heart block (dissociation of atrial and ventricular contractions). Several studies have demonstrated that the G wave is related to the third component of the first heart sound as shown in Figure 2.4, which corresponds to the beginning of mechanical ventricular systole (opening of semilunar valves) [2].

2.3.2 Systolic group

- **H wave**. It is a relatively small upward deflection associated with heart contraction; it begins 0.02 to 0.03 second after the onset of electrical activation of the ventricles (QRS complex) and its duration varies from 0.05 to 0.07 second (duration of the isometric or pre-sphygmic period of ventricular contraction). There are several interpretations for the H wave: some believe that this wave is due to auricular contraction, others that it is due to the apex thrust of the heart. The most valid explanation, however, is that the H wave reflects forces associated with abrupt deceleration in the blood-flow returning to the heart. The H wave almost terminates with the end of the first heart sound (Figure 2.4); in heart diseases, it may become large in amplitude, equaling or surpassing the height of the J wave [2, 21];

- **I wave**. It is a steep and downward wave associated with ventricular ejection. It occurs early in systole and represents the foot-ward recoil of the body from the acceleration of blood upwards in the pulmonary artery and ascending arch of the aorta [21];

- **J wave**. This is generally the dominant wave of the ballistocardiogram related to ventricular ejection. It is important to note that both right and left ventricles

contribute to the ballistocardiogram in a significant way: the right ventricular component is much larger in inspiration while the left is greater in expiration, therefore it is difficult to dissociate the relative activity effects of two sides of the heart. The J wave normally occurs between 0.22 and 0.26 second after the QRS complex of the electrocardiogram, therefore during the late systole. Some studies show an attempt to calculate the cardiac output from the amplitudes and areas of the I-J waves based on their correlation to ventricular ejection; in fact, they are also called "ejection waves" [21];

- **K wave**. This wave normally precedes the onset of the second heart sound (due to the semilunar valves'closure) by 0.01 to 0.02 second, therefore it occurs almost at the end of the systole. In contrast with I and J waves, the K wave is due entirely to the systemic circulation; in fact, it is caused by blood deceleration in the descending aorta and it is directly proportional to the peripheral resistance [2].

2.3.3 Diastolic group

- **L wave**. It is a relatively slow wave associated with circulatory forces. The L wave has a variable form and amplitude, reaching a plateau rather than a sharp peak, which is below the peak of the J wave [21];

- **M,N** and **O waves**. They have a complex origin and cannot be correlated to any single phenomenon of the blood flow. In general, these waves depend on circulatory forces [21].

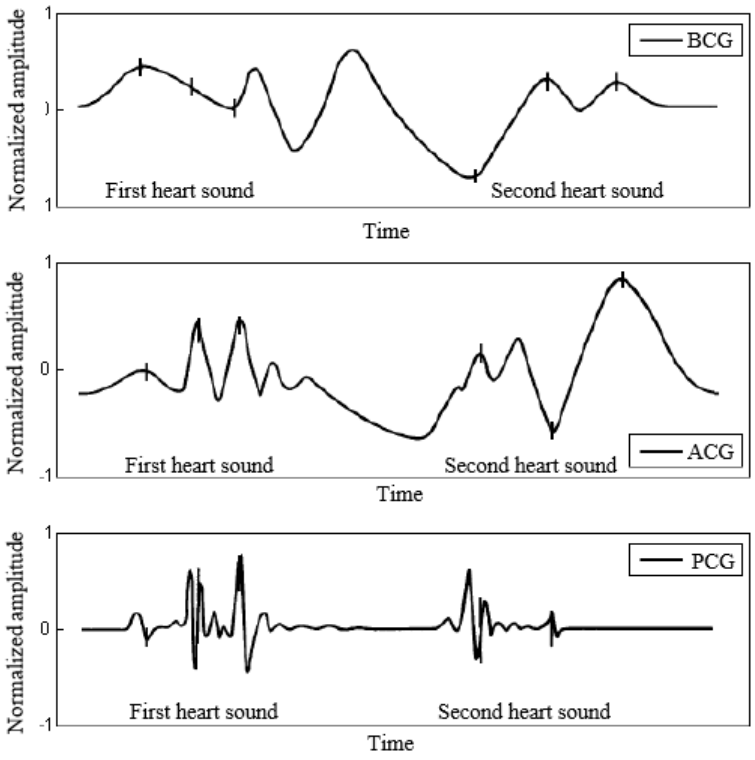

Figure 2.4: Ballistocardiogram, apex cardiogram and phonocardiogram [2]

A healthy subject is expected to have a ballistocardiographic signal similar to the ones presented in Figure 2.2, where the H, I, J, K, and L should be dominant waves forming a W shape [2]. Furthermore, artefacts are easily produced due to the device's architecture, environmental factors, body movements and respiration itself.

2.4 Types of ballistocardiographic systems

The development of new techniques and instruments made it possible to design four different types of ballistocardiographic recording systems, which are:

1. High frequency ballistocardiographic (HF-BCG system);
2. Low frequency ballistocardiographic (LF-BCG system);
3. Ultra-low frequency ballistocardiographic (UF-BCG system);
4. Direct body ballistocardiographic (DB-BCG system).

Each of these systems records the same aspect of motion, for example the displacement, but results may differ in terms of pattern (Figure 2.5) and physical content [25].

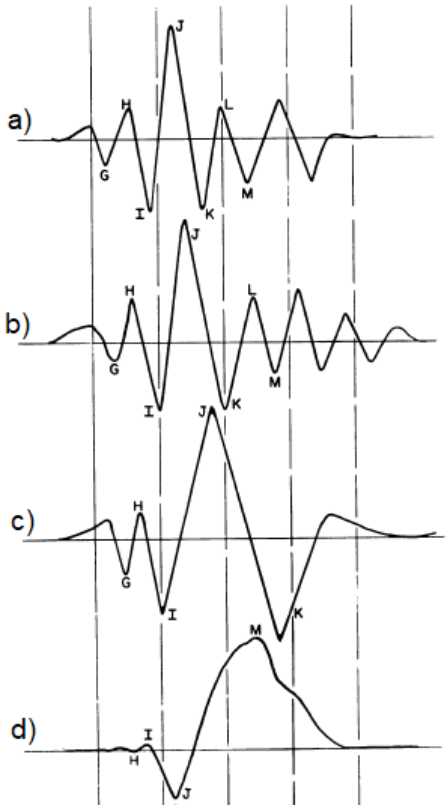

Figure 2.5: Displacement records from HF-BCG system a), DB-BCG system b), LF-BCG system c) and UF-BCG system d) [25]

Ballistocardiographic recording systems consist of a bed, or generally a platform, which provides support for the body. A footboard or other constraints are normally used to increase the coupling between the body and the platform.

2.4.1 High frequency ballistocardiographic system

The reference model of an HF-BCG system is that of Starr. The general characteristics of this system are:

- Platform weights range from 20 lb to 100 lb [1];
- The spring constant of platform to ground is 10-100 times greater than the stiffness of the body's dorsal spring. Typical values are 1000-30000 lb/in and 200-300 lb/in respectively [1];

[1]The measurement units are expressed in the Anglo-Saxon measurement system because they are taken from the article [25]

- The system includes only the damping introduced by the body;
- Loaded with a patient, the fundamental frequency of platform-body system ranges from 3 Hz to 9 Hz.

It is important to note that, unlike other BCG, the high-frequency displacement ballistocardiogram (HF-BCG) does not show fluctuation of the baseline with respiration [25].

2.4.2 Low frequency ballistocardiographic system

One of the first LF-BCG systems was that of Nickerson; its properties are:

- Platform weights are typically the same of the high frequency supports;
- The spring constant of platform to ground is about 1/5 of body stiffness;
- Platform is significantly damped with weight of the subject;
- Loaded with a subject, the fundamental platform frequency is about 1.5 Hz.

The waves of a low-frequency displacement ballistocardiogram (LF-BCG) are designated by the same letters of the HF-BCG; they are in the same direction but significantly later in time. However, breathing causes rather large fluctuations of the baseline which disappear if it is stopped [25].

2.4.3 Ultra-low frequency ballistocardiographic system

Examples of systems that generate an ultra-low frequency ballistocardiogram (UF-BCG) were designed by Gordon, Henderson, Von Wittern, Talbot, Burger and Rappaport. An UF-BCG system is characterized by the following:

- Weights of platform range from 3 pounds to 20 pounds [1];
- The spring constant of platform to ground is only 0.01-0.002 of body stiffness;
- Generally an external damping is used;
- Loaded with a human subject, the frequency of bed-body system ranges from 0 Hz to 0.5 Hz.

The displacement of UF-BCG bears little resemblance to that of other types of BCG because it has a more sinusoidal shape; it is also characterized by absence of faster detail and simplicity of waveform. In fact, there are only two major waves: J-wave, a foot-ward wave that appears in mid-systole, and M-wave, a head-ward wave that appears in early diastole. After the latter, there is a slight foot-ward deflection followed by a progressive

return. Additionally, respiration causes baseline fluctuations but if it is suspended, the baseline usually stabilizes. In contrast to the high and low frequency systems, there are corresponding waves in the acceleration and velocity recordings which are in accordance with the standard BCG nomenclature. In Figure 2.6, a double and single apex are used respectively to distinguish displacement and velocity waves from acceleration waves [25].

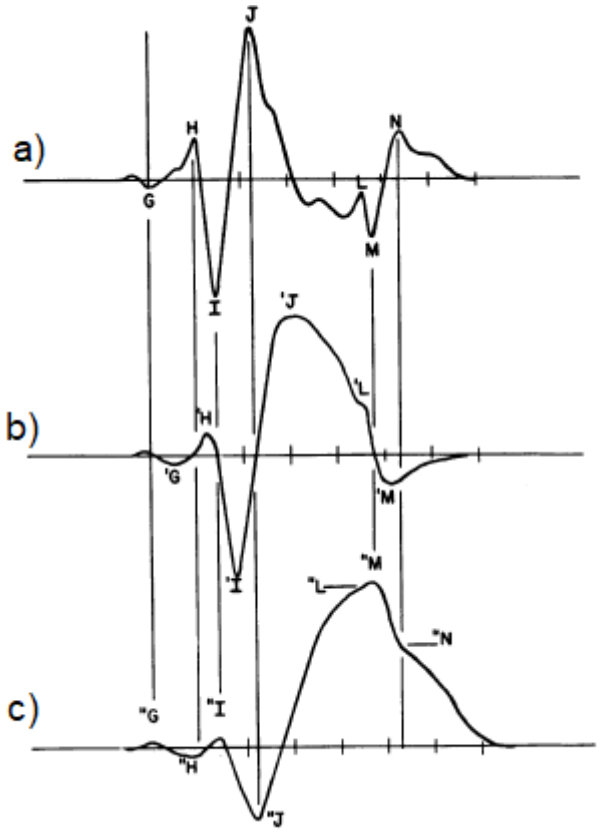

Figure 2.6: Acceleration a), velocity b) and displacement c) ballistocardiogram from an ultra-low frequency system [25]

2.4.4 Direct Body Ballistocardiogram

Recording systems of a direct body ballistocardiogram (DB-BCG) do not include a spring coupled platform but the subject is typically reclined on a surface. For this reason, the mechanical properties of this type of recording system are those of the human body. In detail, the spring constant and damping depend on:

- The type of surface used (e.g. rubber, hard surface, sand);
- The type of body support (e.g. pillow for the head);
- Location and nature of constraints (e.g. footboard or head supports).

The displacement waveform recorded with this system is quite similar to that of a HF-BCG but slightly delayed; however, there is respiratory baseline weave. Moreover, as for the UF-BCG, there are corresponding velocity and acceleration ballistocardiograms [25].

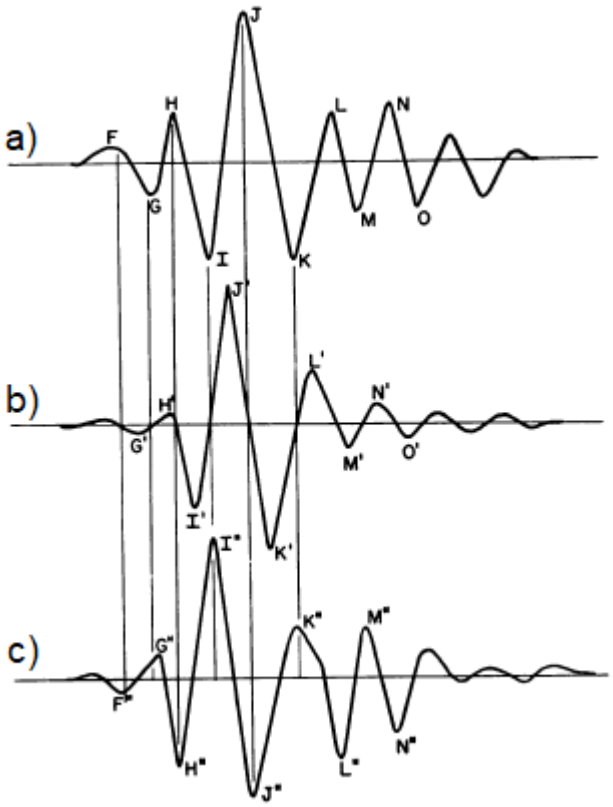

Figure 2.7: Displacement a), velocity b) and acceleration c) ballistocardiogram from a direct body system [25]

The acceleration of DB-BCG is characterized by a quicker detail (e.g. slurring and notching) and is more susceptible to environmental vibration. Furthermore, the acceleration BCG waves are the same as the displacement BCG waves: they are synchronized in time but opposite in direction. As for the velocity recording, the acceleration DB-BCG has a waveform similar to that of displacement DB-BCG but it contains faster detail and its waves are earlier in time.

2.5 BCG signal modelling

Ballistocardiogram modeling is important to better understand the origin of the BCG waves. To do this, some studies focus on the properties of recording systems to understand the effect of these instruments on signal morphology, others instead study the internal forces of the human body that cause its movement [8].

2.5.1 Modeling the recording BCG devices

Over the years, several recording systems were used to record BCG signals, from beds suspended from the ceiling [26] to tables strongly coupled to the ground [27]. However, each of them gave different signal recordings, then efforts were made for modelling the effect of these devices on the BCG signal morphology (Figure 2.8).

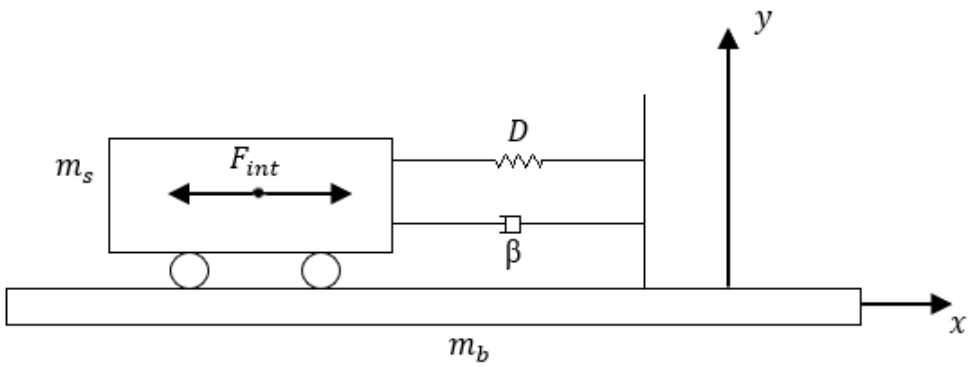

Figure 2.8: BCG recording system modelling

Considering only the head-foot direction (x-axis), the equation that describes the modelling recording system is:

$$(F_{int})_x - \beta\dot{x} - Dx = (m_s + m_b)\ddot{x} \tag{2.1}$$

Where:

- F_{int} is the result of the internal forces;
- β is the damping coefficient;
- x is the body displacement;
- $\dot{x}$ is the velocity;
- $\ddot{x}$ is the acceleration;
- D is the spring constant;
- m_s is the mass of subjects;
- m_b is the mass of recording device.

According to the second principle of the dynamic $(F_{int})_x$ is:

$$(F_{int})_x = m_s \cdot \ddot{x}_c \tag{2.2}$$

Where $\ddot{x}_c$ is the acceleration of the center of body mass. Substituting $(F_{int})_x$ in the equation (2.1), it becomes:

$$(m_s + m_b)\ddot{x} + \beta\dot{x} + Dx = m_s\ddot{x}_c \tag{2.3}$$

From the formula (2.3) three different equations can be obtained. The first is:

$$(m_s + m_b)\ddot{x} = m_s\ddot{x}_c \tag{2.4}$$

It describes a UL-BCG system, i.e. a system weakly coupled to the environment in which the movements of the bed and body are proportional to those of the center of gravity.

The second equation describes the LF-BCG:

$$\dot{x} = \frac{m_s}{\beta}\ddot{x}_c \tag{2.5}$$

Finally, the third equation defines a HF-BCG, which is obtained from a recording system strongly coupled to the environment. This means that the resonance frequency of the recording system is higher than heart frequency. It is:

$$x = \frac{m_s + m_b}{\beta}\ddot{x}_c \tag{2.6}$$

2.5.2 Modeling the internal forces

Starr and his colleagues constructed a model of human arterial tree using an UF-BCG system and based on the physical principle of the BCG signal. Therefore, the arterial tree was divided in 115 segments, the position of the body center was calculated in the longitudinal direction and in each segment by numerical integration of the products of the distance x_i (which is the distance between the center of each segment and the reference plane) and the excess masses during the interval t [8].

2.6 Sources of distortion of the BCG signal

The ballistocardiography is affected by several artifacts some of which are based on the same physical principles, thus it is difficult to distinguish them from the BCG signal. In particular, body movements and breathing are connected with ballistocardiogram baseline fluctuations. For most types of ballistocardiograms, the baseline may be defined as a "neutral" line indicating the position of the body when it is not moving still [25]. *Scarborough* made an interesting observations regarding this aspect, in fact he observed that a relatively flat baseline is often seen in late diastole, when the body's oscillations are minimal or have ceased. Actually, body's motions are always present, then flat baseline is not achieved. Nonetheless, reducing patient motions helps stabilizing the BCG baseline [2]. Regarding breathing, it distorts the BCG signal because the cardiac and respiratory components have overlapping spectra in the frequency domain. In particular, normal breathing causes a slight variation of the systolic BCG wave amplitude, known as ballistocardiographic respiratory variation (BRV). For example, the amplitude of the J wave increases with the onset of inspiration while decreases during expiration. As a consequence, a healthy subject, without moving, will not be able to produce a ballistocardiographic repeatable pattern, even if he accurately controls his respiration. Furthermore, sleep recordings have shown that the BRV increases with heavy snoring and decreases with apnea episodes [28]. Other sources of distortion are floor vibrations, muscular tremors, compliance of body structures, health state and subject's other physical characteristics. For examples, when arrhythmic events are present, as tachycardia, it is difficult or impossible to interpret the ballistocardiographic signal because there is a superimposition among waves that reflect diastole and waves that reflect early systole. Smoking also affects the ballistocardiogram; for instance large diastolic waves are commonly observed in a positive cigarette test [2, 25]. Moreover, if a subject is in lying position on the bed, the BCG signal is influenced by the properties of the mattress and clothes. It should be considered that the gravity force and any contact of the body with external objects impede body movements induced by the recoil forces; consequently, the BCG measured on Earth is always affected by some dis-

tortion. The ideal environment to assess the ballistocardiographic signal would therefore be micro-gravity [8].

2.7 Clinical interest of ballistocardiography

The great inter-subject variability of the ballistocardiogram impairs its use as a diagnostic tool to evaluate a patient's cardiovascular state. However, its intra-subject variability is low, unless there is a change in the cardiovascular state. As a result, in the past ten years the BCG has been proposed as a tool for monitoring these subjective changes. Moreover, it provides information on fundamental aspects of the heart, particularly on its strength [19]. Some studies have been conducted to associate morphology of the ballistocardiographic signal with cardiac disorders. For example, it has been seen that the I-J amplitude is influenced by marked valvular diseases because the velocity and quantity of blood ejection change. In particular, the I-J amplitude decreases with a stenotic mitral valve and if the stenosis is marked, the J-peak may be delayed. However, the I-J stroke rises in aortic failure because stroke volume and velocity of left ventricular ejection increase. On the other hand, hypertension, arteriosclerosis and abnormalities in aortic flow change the K wave. Rheumatic heart disease, constrictive pericarditis, arteriovenous aneurysm and an abnormal return flow to the heart increase the amplitude of H and diastolic waves. Another parameter of great interest is the R-J interval (Figure 2.9), which is the time interval between the R-peak of ECG and J-peak of BCG [21].

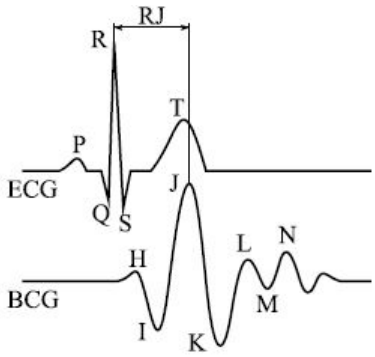

Figure 2.9: Single-beat ECG (top) and BCG (bottom) with the R-J interval [29]

It represents the time elapsed from the ventricular electrical activation to the beginning of cardiac contraction; thus it has been proposed that the R-J interval estimates the cardiac contractility and the systolic blood pressure [30]. Typically, in rest conditions, this interval lasts 180-240 ms but, with paced respiration and hemodynamic changes generated for example by Valsalva's maneuver, it may last from 150 ms to 300 ms [29].

2.8 Conventions of ballistocardiographic systems

The BCG signal can be recorded with different sensors which can be positioned in several points of the acquisition system. In the interest of uniformity of recording, standard spatial axes and conventions of polarity were identified. In particular, the three main body axes were associated with the translational BCG signal recordings [25]:

- **Transverse axis** (side to side): rightward positive and leftward negative;
- **Longitudinal axis** (head-foot): head-ward positive and foot-ward negative;
- **Dorsoventral axis** (anteroposterior): dorsal positive and ventral negative;

These are the most common BCG components that can be obtained in horizontal (including supine, left side, right side and prone positions), standing and seated positions. However, longitudinal direction is the principal component of the BCG signal because it best reflects the major forces of the cardiac contraction [21]. Moreover, the transverse BCG component is highly variable. With regard to the ballistocardiography recording rotations, three orientations referring to the aforementioned three axes are identified [25]:

- **About the transverse axis**: Clockwise positive and counterclockwise negative;
- **About the longitudinal axis**: Clockwise positive and counterclockwise negative;
- **About the dorsoventral axis**: Clockwise positive and counterclockwise negative.

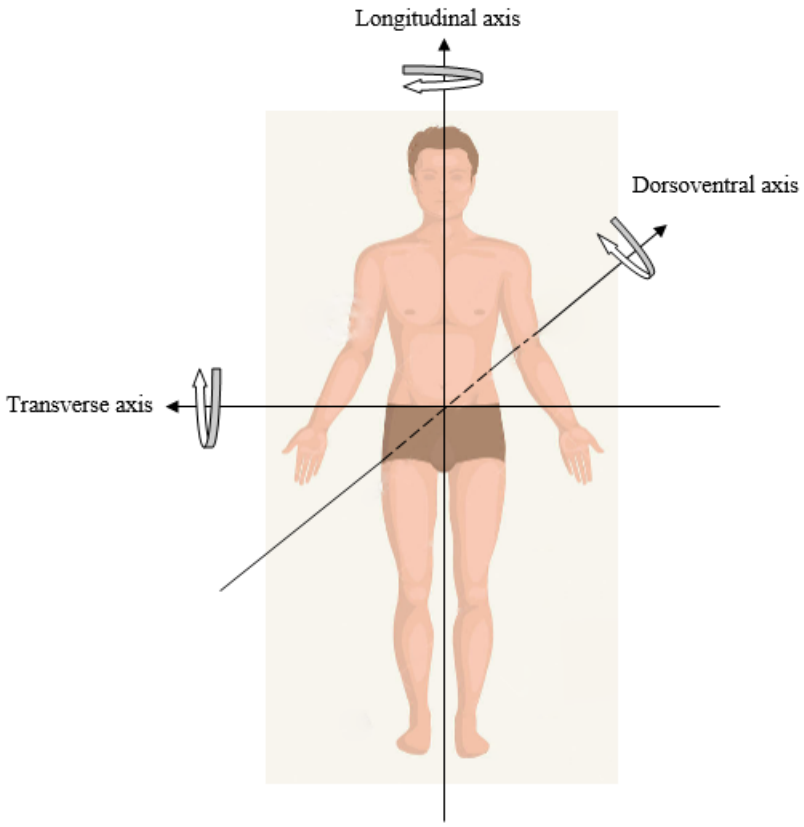

Figure 2.10: Ballistocardiographic axes and conventions for polarity

Sensor location has a fundamental importance since it influences relevant features of the BCG signal, such as morphology and amplitude.

Chapter 3

State of the art

Ballistocardiography is a technique from which information on cardiorespiratory activity can be obtained. As discussed in Section 2.6, the BCG signal is very sensitive to measurement conditions and its morphology changes for each individual. This characteristics makes the detection of vital signs a difficult task in term of signal processing. Various sensors and algorithms have been proposed in literature to record and interpret the BCG signal; the typical physiological parameters extracted are heart rate, heart rate variability, breathing rate, blood pressure and body movements. One of the main advantages of ballistocardiography is its accessibility, which allows the installation of the measurement system in users' homes without affecting their daily activities and their privacy [31]. The sensors, in fact, can be integrated into commonly used objects.

3.1 The modern BCG systems

Over the years, BCG measurement methods have been renewed by replacing the awkward instrumentation with integrated systems; in fact, the development in the electronics sector has made available various sensors for recording the BCG signal. Therefore, researchers have developed modern technologies that could be grouped into three categories: wearable measurement systems, chair and bed-based systems (in the chairs-based system the sensors are typically installed in the seat or backrest while in the bed-based system the sensors are typically installed under the pillow, bed linen or mattress) and weighing scales [17].

3.1.1 Wearable BCG systems

Wearable BCG systems are mainly based on accelerometric sensors that are usually attached to the body (i.e. to the head or chest). The principle of this approach is to detect the acceleration that comes from the body recoil due to the heartbeat.

The accelerometric sensor

An accelerometer is a sensor based on Newton's second law. It is one of the most used sensors for BCG application because it is non-invasive, small and low-cost. An accelerometer is typically modeled as a mass-spring-damper system, as shown in Figure 3.1 where:

- m is the mass;
- k is the spring constant;
- β is the damper coefficient;
- x is the mass displacement.

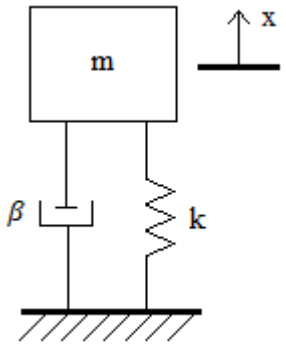

Figure 3.1: Mass-spring-damper model of an accelerometer

In static condition, according to the Newton's second law, the equation that describes the mass-spring-model is:

$$k \cdot x = m \cdot a \tag{3.1}$$

From equation (3.1), the mass displacement is equal to:

$$x = \frac{m \cdot a}{k} \tag{3.2}$$

It is thus possible to obtain the acceleration a from the equation (3.2) by measuring the displacement x. Accelerometers can allow both wearable and non-invasive monitoring, but are highly sensitive to motion artifacts. Therefore, some of their technical specifications must be carefully chosen: they need to be able to record low-frequency and small amplitude movement signals. In particular, as mentioned in the Section 1.4, the ballistocardiographic cardiac component amplitude is of the order of mg while the ballistocardiographic respiratory component amplitude is even lower, i.e. 0.1 mg. The ability of an accelerometer

to detect these signals depends on a technical specification called minimum detectable acceleration or resolution (a_{min}). Assuming that an acceleration is detectable when it can generate a voltage larger than the accelerometer noise, a_{min} is given by the following relation [32]:

$$a_{min} = \frac{Noise\ voltage}{Sensitivity} \tag{3.3}$$

As a consequence, a high sensitivity is required to detect a small acceleration. Another characteristic of accelerometers is the noise floor, which must be low. It is determined by the thermo-mechanical noise [32]:

$$\frac{a_{min}^2}{f} = 4K_B T \omega_0 \frac{1}{mQ} \tag{3.4}$$

Where:

- f is the accelerometer bandwith, i.e. the frequency range in which the sensor operates;
- K_B is the Boltzmann constant;
- T is the temperature;
- ω_0 is the resonant frequency (angular);
- m is the proof mass;
- Q is the quality factor.

From the equation (3.4) it is possible to infer that the resolution a_{min} improves with low frequencies; consequently, the noise can be partially suppressed by limiting the accelerometer bandwidth f. Moreover, the resolution improves even with high values of m because the proof mass is inversely proportional to a_{min}. However, to reduce the discomfort related to the use of these devices, it is preferable to have sensors of reduced size and weight. A heavy weight accelerometer may also cause the undesired mass loading effect [32]. In this regard, the micro-electro-mechanical systems (MEMS) accelerometers have an advantage over the other conventional ones; in fact they have reduced dimensions due to the manufacturing technique used. The MEMS accelerometers integrate both mechanical parts and electronic conditioning and control circuits in a single silicon chip and they typically have a noise floor in $mg/\sqrt{Hz}$. Over the years the characteristics of these sensors have been improved: they have become smaller, less intrusive and cheaper and have reduced their power consumption [33]. As can be observed in equation (3.2), a small

mass is not favorable to achieve good sensitivity and consequently a low a_{min}; in fact, the detection of the BCG signal with MEMS accelerometers is a challenge [32]. The left side of equation (3.4) is the squared noise density. The noise density can be found with the following equation:

$$N = \frac{a_{min}}{\sqrt{f}} \tag{3.5}$$

Finally, the upper end of the bandwidth is generally limited by the natural frequency of the sensor f_0:

$$f_0 = \frac{1}{2\pi}\sqrt{\frac{k}{m}} \tag{3.6}$$

It can be seen from equations (3.2) and (3.6) that, when the mass is fixed, there is a link between the bandwidth and the accelerometer sensitivity: using an accelerometer with a bandwidth wider than needed is not indicated since the sensitivity worsens [32]. This category of sensors is also used to detect the SCG signal, but it is important to note that the low-frequency components of the accelerometric signal (0.6 - 20 Hz) are related to the BCG, while the high-frequency components (>18 Hz) are related to the SCG [17].

3.1.2 Chair and bed-based BCG systems

The measurement modality of the bed-based BCG systems, normally used for monitoring vital signs in bedridden subjects and for sleep studies because they do not cause discomfort to sleep and do not require any user action, is similar to the original BCG systems [14]. The quality of the data acquired with these systems depends on materials and thickness of the mattress [34]. Chair-based systems are instead convenient for subjects who cannot stay still on their own or for non-ambulatory patients [17]. The sensor used in these type of recording systems, in addition to the accelerometers, are the following:

- **Strain gauges**. They are force sensor consisting of a reflex light barrier inserted between two aluminum plates [31]. When a force is applied to a strain gauge, the two aluminum plates are compressed and the distance between them diminishes. Thereafter, the reflex light converts the distance reduction into a voltage signal which is subsequently pre-amplified and passed through a low-pass filter to reduce noise and ripple. Strain gauges detect the BCG signal out of the bed plane, they are generally in a Wheatstone bridge configuration and are typically positioned under the bedposts or on the bed frames. It is interesting to note that the sensors situated under the bedpost are more prone to interferences than the sensors placed under the monitored subject due to the movements of other persons [4]. *Load cells* are another

category of force sensors based on strain gauges; they are typically installed under the bed supports.

- **Capacitive sensors (Electromechanical film sensors-EMFi)**. An EMFi sensor is a thin and elastic bi-axially oriented polypropylene film covered with electrically conductive layers. It has static charge of hundreds and some air voids separate the polypropylene layers [31, 35]. When a force, or an external pressure, is applied to the surface of the film, the thickness of the air voids changes. This causes the movement of the charges located on the polypropylene-vacuum interface, thus the EMFi sensor transforms this mechanical energy in an electric signal. The electrical signal is weak, therefore it needs to be pre-amplified. The EMFi sensor is usually used in chair-based systems and measure both out-of-plane and longitudinal BCG signal.

- **Piezoelectric sensors**. The piezoelectric effect is the capacity of some materials to produce an electric charge when they are subject to mechanical stress. One of the most suitable materials to detect the small fluctuations generated by body is the polyvinylidene fluoride (PVDF); it is an elastic, thin and permanently charged semi-crystalline piezoelectric film that creates an external electrical field if a pressure force is applied to it [31]. A piezoelectric sensor then records ballistic forces of the heart and converts them to electric impulses.

- **Fiber optic-based sensors**. The principle of these systems is to measure the change in length of the optical fiber due to the cardiorespiratory activity with an optical interferometer [36]. In literature it is possible to find several ballistocardiographic systems based on the micro-bend fiber-optic sensors (MFOS) and the fiber Bragg grating sensors (FBGS). In particular, the MFOS consists of a multimode optical fiber clamped between a pair of micro-bends. The displacement between two micro-bends, due to cardiorespiratory activity, changes the light intensity in the micro-bending fiber and the heart and breathing rates can be obtained by demodulating the sensor output signals [31, 37]. It should be noted that some light is dispersed through the fiber walls but, if an optical fiber is bent, the amount of light lost is insignificant. The FBGS instead act as a filter for a specific wavelength of light; they detect the reflected wavelength shift due to changes in pressure, temperature or mechanical strain [38]. Unlike electrical sensors, fiber-optic sensors are immune to electromagnetic and radio-frequency interference [31] but the high cost limits their use for BCG recording.

- **Pneumatic-based sensors**. The pneumatic system consists of a thin air-sealed cushion insert between the mattress and bed. When a person rests in the bed,

the forces derived from respiration, heartbeat and body movements cause a pressure, which can be measured with a super-sensitive pressure sensor. Several studies demonstrated that the pneumatic-based sensors are more sensitive to environmental noise, such as door opening and closing [31].

- **Hydraulic-based sensors**. They are normally placed under the mattress and measure the change in pressure applied to a liquid-filled tube [31]. These changes are then converted into an electrical output signal. The hydraulic sensors are low cost, flexible and easy to use.
- **Optical sensors**. They are a solution for bed-based systems and includes an infrared light source and a photodetector: the former emits light into the mattress while the latter records continuously the intensity of the light scattered back due to the deformations of the mattress caused by the cardiorespiratory activity and cardiac body movements [39].

The advantages of chair and bed-based systems are the comfort of the user, the reduction of motion artifact and the possibility of easily integrating them into the home environment. Some potential drawbacks are postural effects on the signal integrity, the unintentional combination of transverse and longitudinal BCG components and, in the case of the chair-based systems, the reduced signal amplitude [17].

3.1.3 Weighing scale-based BCG systems

BCG measurement on electronic weighing scale was first discovered at the Linear Technology Corporation by *Williams*. He noted that, when a subject was on an ultra-precise electronic scale, there was a "noise" in the measurement synchronized to the subject's heartbeat, this "noise" was the BCG signal. The advantages of weighing scale-based BCG systems are the repeatability of measurement and the easy availability of weighing scales at home. Furthermore, the weighing scales are already utilized for heart failure patients to control their fluid status changes. Nevertheless, motion artifacts and postural variations in the measurement can affect the signal integrity. Another disadvantage is the limited measurement duration because the subject must stand still for so long [17].

3.2 BCG signal processing methods

The BCG signal is strongly influenced by motion artifacts and other environmental factors, thus in almost all algorithms a pre-processing step is present for extracting the cardiac and respiratory components in the right frequency range. The most used filter for this purpose is the Butterworth band-pass filter. It is known that the cardiac component is located between 0.5-20 Hz frequency range while the respiratory component is located in a frequency range less than 0.5 Hz. After filtering, one of the following methods is used to extract vital signs of interest. Processing and interpretation of the BCG signal can be generally performed with time-domain algorithms, frequency-domain algorithms and time-frequency analysis.

3.2.1 Time-domain algorithms

Time-domain algorithms are focused on identification of heartbeats (signal maxima) using a moving window, which is an array consisting of a certain number of samples values continuously copied from signal [40]. As its name implies, the moving window moves along the acquired signal sample by sample, extrapolating only the signal portion of interest (i.e. the cardiac cycle). The optimal size of the moving window depend on both the sample rate and the range of frequency to be detected. After identifying J-peaks locations, J-J intervals (i.e. the time between two successive heartbeats) are determined.

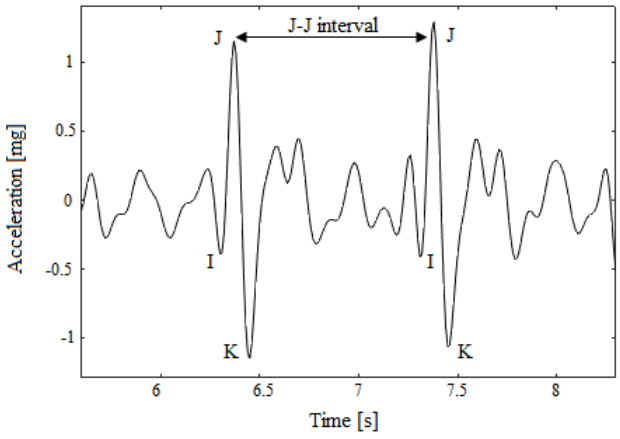

Figure 3.2: The J-J interval

Heart rate is then calculated with the following formula:

$$HR = \frac{60}{J\text{-}J\ interval}\ [bpm] \tag{3.7}$$

Time-domain algorithms are generally preferable because they consider the HRV; however, since the BCG signal is a non-linear and non-stationary one, detection of beat-to-beat intervals is a hard task due to motion artifacts, the variability of ballistocardiogram and its less-pronounced peaks [14]. Therefore, the accuracy of these approaches may not be high. Several methods were proposed to find heartbeat locations from BCG signal; one approach, for example, is to detect the I and J waves, which usually correspond to the largest negative and positive deflections of each heartbeat [41]. Another algorithm used in literature is based on the use of an adaptive threshold, evaluated as a certain percentage of the maximum value found in the moving window. The value of the adaptive threshold decreases moving away from a detected maximum. The autocorrelation function can also be used to estimate heart rate in time-domain. In particular, the output of the autocorrelation function is first smoothed and differentiated in order to emphasize the signal peaks; then the HR is computed by measuring the intervals between two peaks of the autocorrelation function. Finally, unsupervised (e.g. cluster approach) and supervised (e.g. multilayer perceptron) machine learning algorithms have been implemented for detecting J-peaks locations [31]. Specifically, the cluster approach (CA) is a method of organizing a set of data (training set) in groups, called clusters, based on similarity measures (training step); in fact, the elements within a cluster are similar to each other and dissimilar to those of another cluster. First, a model for heartbeat shape is constructed and subsequently, the similarity between the heartbeat template and a signal segment is calculated (template matching). If similarity is high, a heartbeat is detected. Examples of CA are the k-means algorithm [14] and the dendrogram [42, 43]. Despite the CA is a very simple and fast procedure, it has one big disadvantage: it is very selective. In fact, the choice of similarity measures and template are critical factors [44]. Moreover, if the algorithm learned the wrong pattern during the training step, all successive heartbeat detection attempts will fail and the number of over-detected or missed heartbeat could thus be high. Additionally, training data set has to be re-initiated every time the heartbeat templates vary, for example due to posture changes [9]. The supervised machine learning methods are instead based on three steps [45, 46]:

1. **Segmentation stage**. In this step the BCG cycles are computed.
2. **BCG signal features extraction**. A method used for this purpose is the Principal Component Analysis (PCA), which reduces the number of signal features and therefore allows to keep the most informative only. The PCA finds the principal components by numerically computing the eigenvectors of the variance matrix. The eigenvectors with largest eigenvalue are the features onto which the data are projected [47].

3. **Classification** of each BCG spike according to the features extracted. To predict if the input BCG segment includes the IJK complex or not, one of the most used methods is the multilayer perceptron (MLP), a feed forward supervised artificial neural network (ANN), requiring a desired response to be trained [46].

Although the supervised machine learning algorithms detect the BCG waveforms robustly, their computational cost is high and they also require simultaneous recording of the ECG signal for the segmentation stage.
Regarding the estimation of breathing rate RR, the previously described methods can be used. The breathing rate is computed according to the following formula:

$$RR = \frac{60}{RCL} \ [bpm] \tag{3.8}$$

Where RCL is the respiration cycle length, i.e. is the time between two successive respiratory peaks (Figure 3.3).

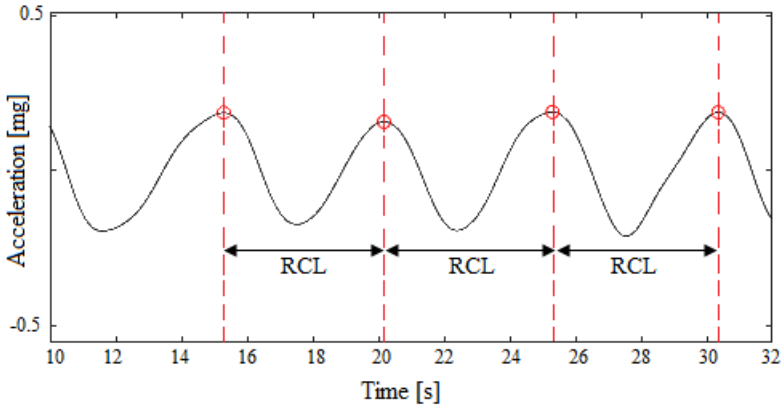

Figure 3.3: Illustration of respiratory signal (in black) and RCL

3.2.2 Frequency-domain algorithms

Frequency-domain algorithms typically extract the periodicity of the BCG signal through the Fourier transform (FT).

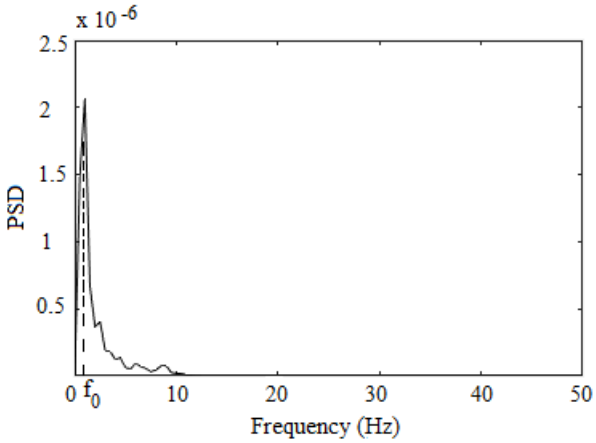

Figure 3.4: Frequency spectrum of the BCG signal

Thereafter, the average heart rate is obtained from the dominant frequency (f_0) of the signal spectrum [34, 48].

$$HR = 60 \cdot f_0 \ [bpm] \tag{3.9}$$

The Hilbert Transform (HT) is also one of the most used operator to identify f_0. It yields a complex output whose real part is the original signal and the imaginary part is the 90-degree phase-shifted signal version [34].

$$HT(t) = s(t) + jm(t) \tag{3.10}$$

The dominant frequency is then extracted from the Fast Fourier Transform (FFT) of the squared magnitude of the HT. Frequency-domain algorithms do not provide information about J-J intervals, i.e. on HRV, and the possible presence of multiple peaks in the signal spectrum can result in an inexact estimation of vital signs [31]. Another interesting technique is based on the use of the signal cepstrum (C_x), which is the real part of the inverse Fourier transform of the logarithm of the estimated signal spectrum (S_x).

$$S_x = F\{x\} \tag{3.11}$$

$$C_x = real(F^{-1}\{log_e(|S_x|)\}) \tag{3.12}$$

The logarithm of the BCG signal spectrum consists of peaks at the harmonic frequencies of the fundamental heartbeat frequency. In the cepstrum, spectrum periodicity is represented as a peak located at the time point that corresponds to the time interval of two heartbeats. The cepstrum is a useful approach in the case of signal with quasi-periodic trend, but strongly variable; however, it has two disadvantages, namely the high variability of the signal spectrum and the low resolution of the cepstrum due to averaging between the successive time windows [49]. The HT, PSD and cepstrum can also be used to detect the breathing rate.

3.2.3 Time-frequency analysis

Time-frequency analysis is generally used to process variable frequency signals. As its name implies, it describes, through the use of functions, the energy density of a signal both in time and in frequency in one graphic and analytical representation: the x-axis representing the time, while the y-axis representing the frequencies contained in the signal. One common approach for estimating a time-frequency distribution (TFD) is the Short-time Fourier Transform ($STFT$). In the STFT the signal *x(t)* is divided into small records, each of which is assumed to be stationary. Subsequently, each record is multiplied by a fixed window function $\omega(\tau)$ and finally, the FFT is applied to each record [50].

$$STFT\{x(t)\}(\tau,\omega) = \int_{-\infty}^{+\infty} x(t)\omega(t-\tau)e^{-j\omega t}dt \tag{3.13}$$

After the $STFT$ calculation, an algorithm is used for detecting the heart rate extracting local maxima of the $STFT$ envelope [51]. This type of time-frequency distribution is relatively simple but, since there are signals for which the approximation of stationary signal may not be valid for any record, it may not track the rapid frequency changes over time effectively. For this reason, the window function $\omega(\tau)$ should be as short as possible. This, however, will reduce the resolution in the frequency domain. In fact, the $STFT$ has a static resolution because improving the resolution of either frequency or time domain worsens the resolution in the other domain [50, 52]. The Wavelet Transform (WT) was suggested to improve the resolution both in time and frequency domains; in fact, unlike the $STFT$ that uses the same window at low and high frequencies, the WT uses short windows at high frequency and long windows at low frequency. The objective of the WT is to decompose the raw signal into low and high-frequency components [31], and the component with a good agreement with cardiac (or respiratory) component is then selected. Subsequently, applying a simple peak detector, the inter-beat intervals can be found. The Wavelet theory can be divided into two parts: The Continuous Wavelet Transform (CWT) and the Discrete Wavelet Transform (DWT). While the former is often

used for signal time-frequency analysis, the latter is more useful for denoising and signal filtering. In particular, the CWT of the signal x(t) is defined as follows (equation 3.14) [52]:

$$X_{WT}(a,b) = \frac{1}{\sqrt{a}} \int_{-\infty}^{+\infty} x(t)\bar{\psi}\Big(\frac{t-b}{a}\Big)dt \tag{3.14}$$

Where $\bar{\psi}$ is the complex conjugate of the mother wavelet (ψ), which is a continuous function in both time and frequency domains. An advantage of this procedure is the absence of a filtering step because it is implicitly done when the CWT is computed. An alternative approach of Wavelet analysis to process non-linear and non-stationary signals is the Empirical Mode Decomposition (EMD); it decomposes the signal into so-called intrinsic mode functions (IMFs) with separate spectral band and without prior knowledge. Each mode function has local maxima and minima that are all positive and negative respectively. The IMFs, found by an iterative method called the sifting algorithm, can be analyzed with the HT. The EMD has some disadvantages. It is affected by mode mixing (i.e. the inability to separate the mode in a single IMF, thus it remains mixed in another IMF. This limit is due to the presence of interferences or to presence of closely spaced spectral components [53]). Its accuracy is not very high and its computational complexity is elevated, thus the input signal length is limited. To try solving the mode mixing problem, the Ensemble Empirical Mode Decomposition (EEMD) and the Complete Ensemble Empirical Mode Decomposition with Adaptive Noise (CEEMDAN) were suggested. The EEMD is a noise-assisted data analysis (NADA) method that adds a white noise of finite amplitude to signal and then determines the true IMFs [54]. Nevertheless, it is characterized by a low decomposition efficiency, an ineffective extraction of fault features and it has many pseudo-components. The CEEMDAN instead adds an adaptive white noise in each decomposition stage [55]. However, the computational cost of the EEMD and the CEEMDAN methods is high and they do not completely solve the mode mixing problem. The most used methods for detecting the breathing rate in the time-frequency domain are the $STFT$ and the WT [56, 57].

Chapter 4

The proposed algorithm

The acquired data not only include the BCG components of interest (i.e. the cardiac and respiratory signals) but also contains environmental noise and motion artifacts; consequently, in order to clean up the heartbeat BCG waveforms from the out-of-band components, a signal processing algorithm is necessary. The algorithm proposed in this thesis is applied to BCG signals acquired through an accelerometer incorporated in a bed-based recording system (whose details are covered in Chapter 5). In particular, the presented method is implemented in the time domain because, although the performance of this category of algorithm is limited by the high variability of ballistocardiogram and motion artifacts, as discussed in Section 3.2.1, it provides information about the HRV with respect to the frequency-domain algorithm. In this way, information on HRV could be used to assess the risk of cardiac arrhythmias or factors affecting heart and breathing rates. Furthermore, compared to the time-frequency analysis, time-domain algorithms have a lower computation cost. The block diagram of the proposed method is shown in Figure 4.1. It includes a pre-processing step with the aim of removing the noise contained in the acquired signals; subsequently, the vital signs of interest (i.e. heart and breathing rates) are computed. Moreover, given the non-stationary nature of the BCG signal, due to dynamic cardiac behavior, the algorithm is based on parameters directly derived from the signal itself, thus it can better track heart rate changes.

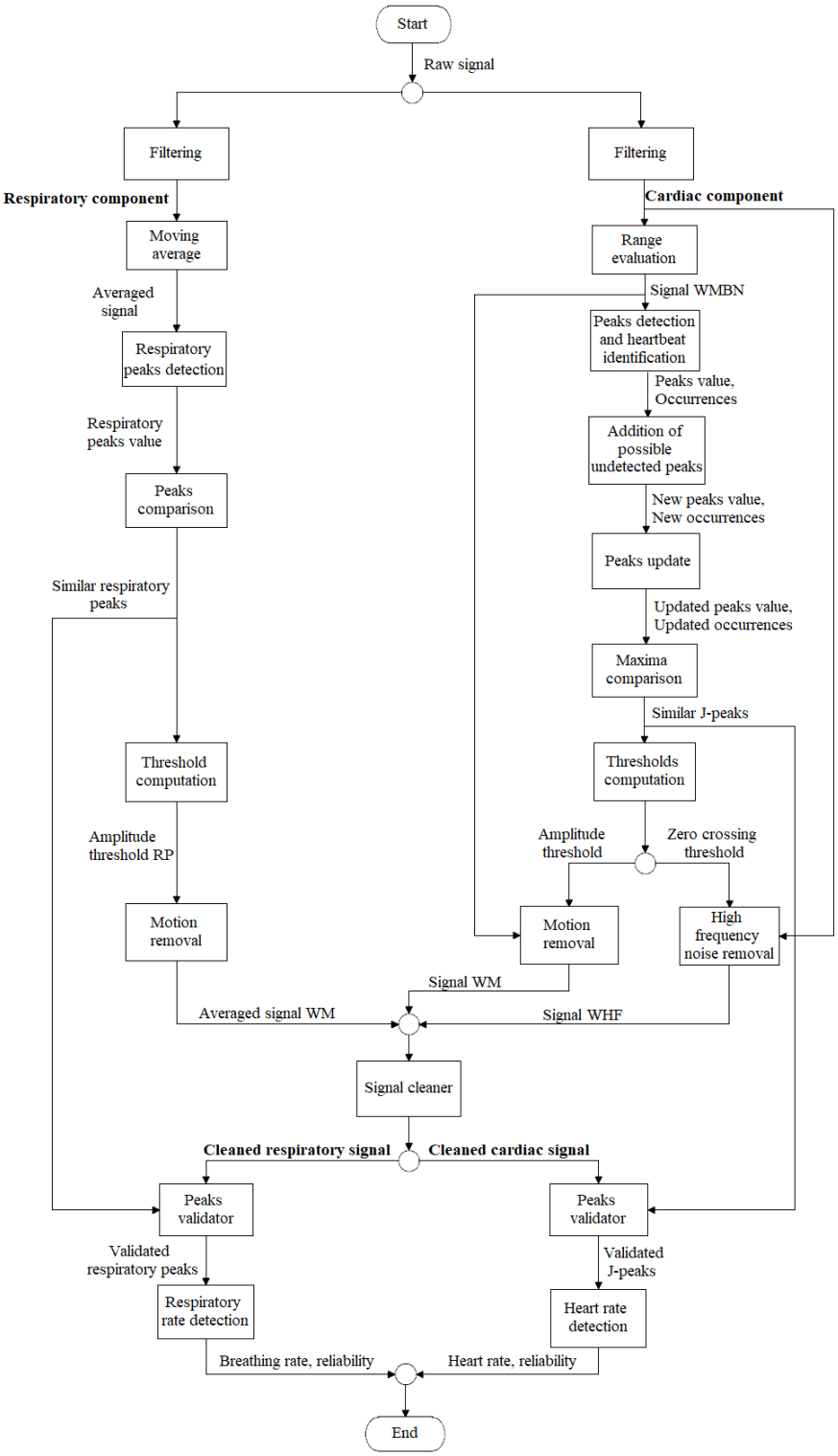

Figure 4.1: Block diagram of the proposed algorithm

4.1 Pre-processing step

Signal-to-noise ratio decreases significantly if there is a high content of out-of-band components; therefore, in this conditions, it is difficult to obtain a reliable estimation of vital signs. The first part of the proposed algorithm, i.e. the pre-processing step, aims to discard the noisy signal segments; it consists of two sub-parts that can be performed in parallel: the extraction of the noise-free cardiac and respiratory components.

4.1.1 Noise-free cardiac component extraction

The raw signal is filtered using a fifth-order Butterworth band-pass filter with cutoff frequencies (derived from the power spectral density of signal) of 0.5-10 Hz in order to obtain the cardiac component. An example of ten BCG pulses extracted is shown in Figure 4.2.

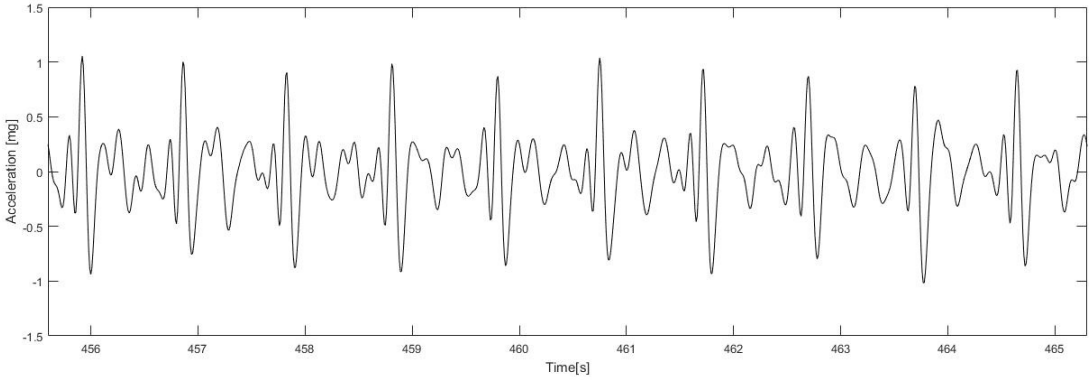

Figure 4.2: Enlarged view illustrating the extracted cardiac component

Range evaluation

The filtered signal consists of multiple components (i.e. cardiac signal, background noise and body movements), thus an evaluation of signal range (i.e. the difference, in absolute value, between the maximum and minimum) is performed using a moving window over a duration of one second[1] with 50% overlap. For each window, the following check is made: if the difference between the maximum and minimum is larger than 8 mg and less than 0.3 mg, the current window is discarded. These values have been derived from the BCG signal range, which is approximately 0 - 7 mg, as mentioned in Section 1.4. In the

[1] 1 second correspond to 100 samples

block diagram the output of this step is "Signal WMBN" which means "Signal Without Movements and Background Noise".

J-peaks detection

A heartbeat detection method is used to detect the J-peaks locations. In general, this type of algorithm identifies the peak candidates with an adaptive threshold that determines the higher peak in a specific region and then removes neighboring small peaks in that region [58]. The proposed method, instead, identifies the moving maximum within a window that moves along the signal sample by sample. The equation 4.1 is the formula to identify the moving maximum signal [58]:

$$m[i] = max(Signal\ WMBN[j]) \tag{4.1}$$

$$j \in [i\text{-}M+1,i]$$

Where:

- **m** is the moving maximum signal at the ith iteration;
- **M** is the sliding window length; its value is 50 samples because the region in which the moving maximum signal is found has been set to 0.5 s. This is related to the value of heartbeat-to-heartbeat interval, which ranges from 0.5 to 1.5 s [58].

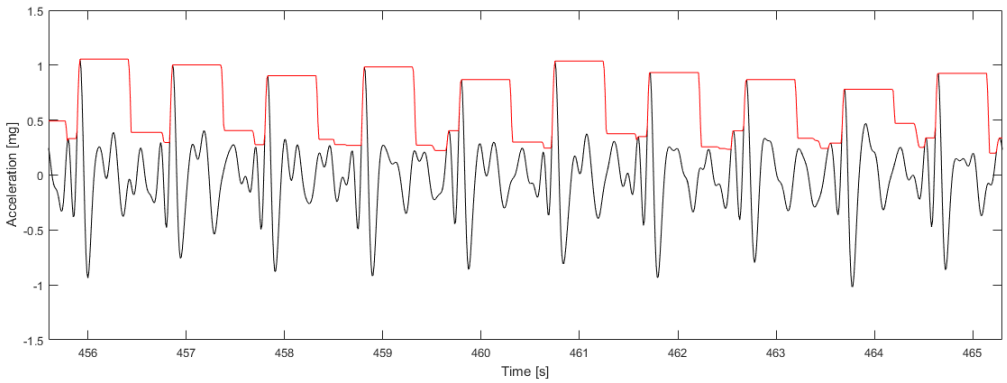

Figure 4.3: Waveform of BCG signal (in black) and its moving maximum signal (in red)

The moving maximum signal forms an upper envelope (Figure 4.3) characterized by a flat trend, in correspondence of a J-peak, maintained for a duration equal to *M*.

The holding time t, which is the duration for which the largest peak is preserved in a specific region, is calculated with the following formula [58]:

$$t[i] = \begin{cases} t[i-1]+1, & \text{if } m[i-1] = m[i], \\ 1, & otherwise. \end{cases}$$

The holding time t increases as long as the moving maximum value remains the same while it is initialized to 1 when the moving maximum values changes, thus t is described by a saw-tooth waveform (Figure 4.4)

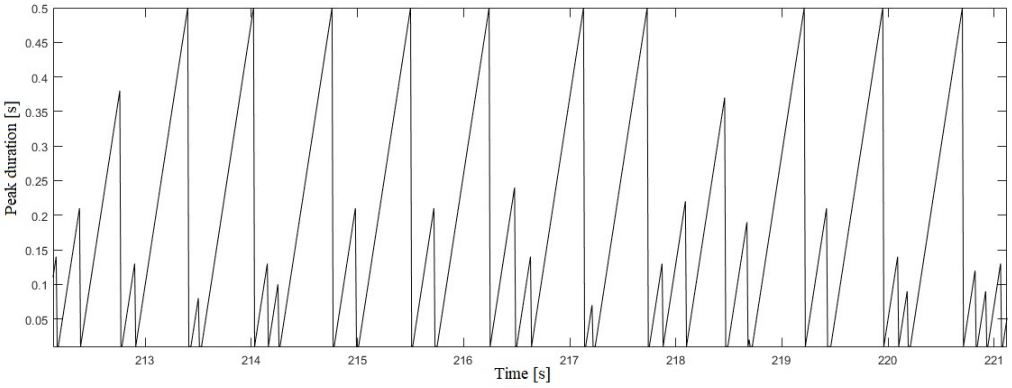

Figure 4.4: The holding time of peaks in the moving maximum signal

A heartbeat is a peak whose holding time reaches M. In particular, the equation with which a peak is classified as a heartbeat b is the following [58]:

$$b[i] = \begin{cases} 1, & \text{if } t[i] = M, \\ 0, & otherwise. \end{cases}$$

Additionally, the heartbeat position is equal to $i - M + 1$ because it is computed after M samples.

Addition of possible undetected peaks and peaks update

Since the total removal of all noise present in the signal is hard due to the high variability of BCG signal, some J-peaks may not be detected. To avoid this, the following check is made: if the current HRV is larger than the one by 25%, the sliding window length is reduced to 36 samples, which correspond to a holding time of 0.36 s. The choice of this value is based on the J-peak duration, which ranges from 0.3 to 0.5 s, as found in literature [58]. Subsequently, **peaks update** was performed.

Maxima comparison and thresholds computation

In order to remove the remaining body movements and the high frequency noise, the differences between two consecutive and two previous J-peaks is performed. If these differences were higher than experimentally obtained values, the three J-peaks were discarded (**Maxima comparison**). In this way, the similar J-peaks are found. Thereafter, two peaks-adaptive thresholds, i.e. the *zero crossing threshold* and *amplitude threshold*, are calculated in a 10-second moving window as the mean and the maximum of the similar J-peaks respectively (**Thresholds computation**).

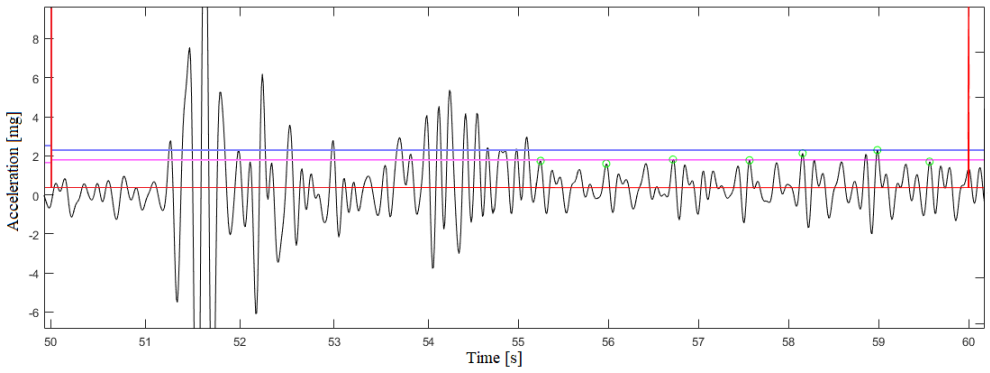

Figure 4.5: BCG signal with sliding windows (in red), amplitude threshold (in blue), zero-crossing threshold (in magenta) and the similar J-peaks (in green)

Motion removal

The remaining body movement were removed comparing each signal sample with each sample of the *amplitude threshold*, calculated in the previous step; in particular, the signal samples above the amplitude threshold are discarded. The output of this step is "Signal WM", which means "Signal Without Movements".

High frequency noise removal

One of the most used method to remove the high-frequency noise is the zero crossing detection technique, which gives a measure of the frequency of the dominant component in a signal segment. In particular, for a low-frequency component there are fewer zero crossings per segment than for a high-frequency component [59]. As shown in Figure 4.6, the cardiac component is characterized by a low number of zero crossings during the IJK complex and a high number of zero crossings during non-IJK segments.

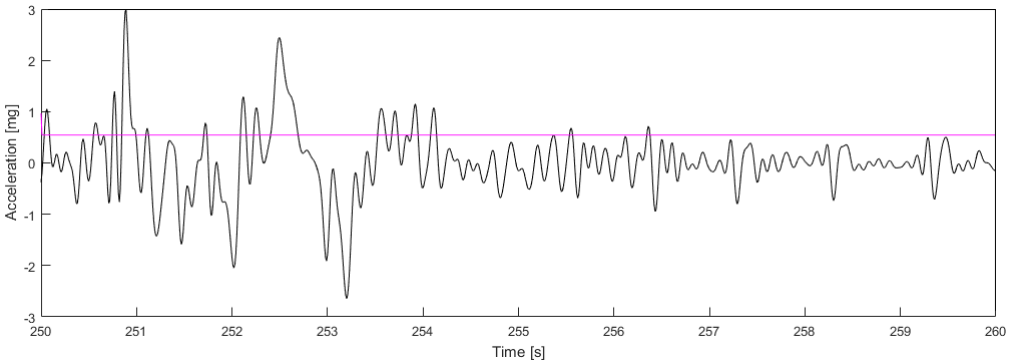

Figure 4.6: Enlarged view of the BCG signal (in black) and the zero crossing threshold (in magenta)

A zero crossing is detected when the signal rises above the *zero crossing threshold*, previously calculated. Subsequently, signal segments containing a number of zero crossing greater than twice the number of similar J-peaks were discarded. The output of this step is "Signal WHF", which means "Signal Without High Frequency".

4.1.2 Noise-free respiratory component extraction

The respiratory component was extracted filtering the raw data with a third-order Butterworth band-pass filter with cutoff frequencies of 0.13 Hz and 0.5 Hz. The cutoff frequencies were derived from physiological breathing rate under resting condition (8-30 bpm).

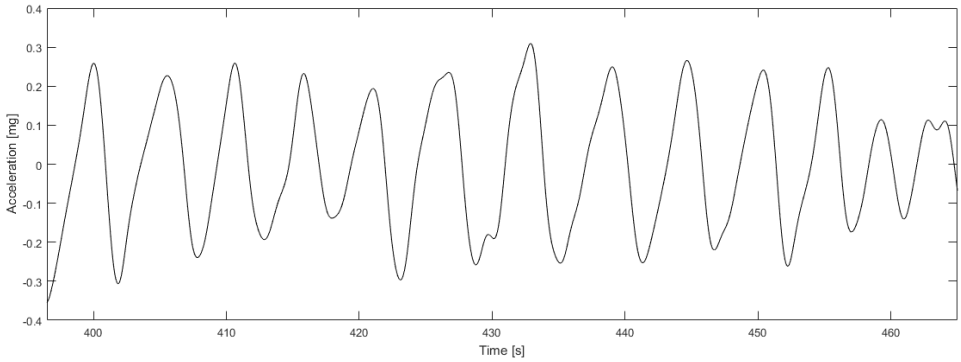

Figure 4.7: Enlarged view illustrating the extracted respiratory component

Moving average

Moving Average (MA) is a widely used statistical indicator to analyze signals. The term "moving" denotes a reference position in space while the term "average" indicates the mean of signal subsets calculated according to the spatial reference. The equation 4.2 is the general function to compute the MA [58]:

$$MA[i] = \frac{1}{N} \sum_{j=0}^{N-1} x[i-j] \tag{4.2}$$

Where:

- $\boldsymbol{N}$ is the length of a sliding window;
- $\boldsymbol{x}$ is the signal;
- $\boldsymbol{i}$ is the iteration.

MA is normally used to smooth signal fluctuation and to reduce the random spike effect. In particular, the greater the sliding window length N the greater the signal smoothing. Mathematically, MA represents a type of convolution, thus in signal processing it can be seen as a low-pass filter. This function has been applied to the respiratory component to avoid multiple peak detection; in particular, the window length N has been set to 1 second to prevent excessive signal smoothing. The MA effect on the respiratory signal is show in Figure 4.8.

Respiratory peaks detection

Respiratory peaks are detected with a peak detection algorithm; in particular, a signal sample is classified as a peak if its 100 previous and successive samples have a smaller amplitude than it.

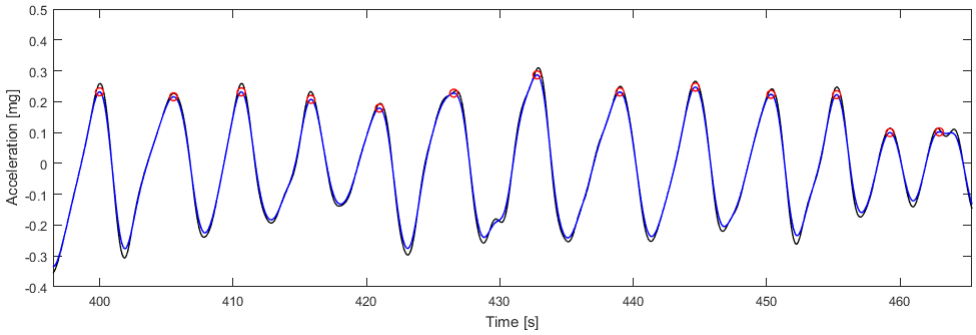

Figure 4.8: Respiratory signal (in black), Averaged respiratory signal (in blue) and detected respiratory peaks (in red)

Peaks comparison, threshold computation and motion removal

In order to remove the motion artifacts still present in the signal after applying the previous steps, the differences between two consecutive and two previous respiratory peaks were computed. Subsequently, the respiratory peaks whose amplitudes differ from others by an experimentally obtained value, are discarded. The similar respiratory peaks are thus found. Thereafter, a threshold (*Amplitude threshold RP*) is computed as the maximum of the all similar respiratory peaks (**threshold computation**) and the signal samples above that threshold were removed (**motion removal**). "Averaged signal WM", which is the output of this step, means "Averaged signal without movement".

4.1.3 Signal cleaner

In the signal pieces affected by noise it is not possible to calculate heart and respiratory rates since the BCG signal is not identifiable. In fact they have been removed by applying the previous steps. Consequently, the signal samples near the discarded signal windows are not reliable for estimating the vital signs of interest. For this reason, the 100 signal samples preceding and following the noisy signal pieces have been removed both from cardiac and respiratory component.

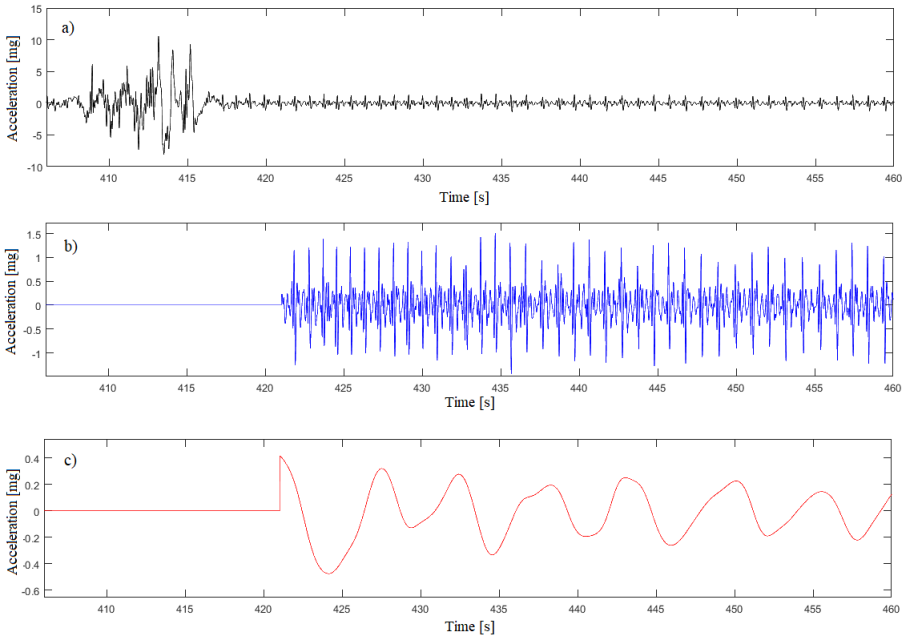

Figure 4.9: Enlarged view illustrating pre-processing result; a) Filtered BCG signal, b) Cleaned cardiac component; c) Cleaned respiratory component

4.1.4 Peaks validator

The final stage of the pre-processing step is the validation of the cardiac and respiratory peaks which consists in discarding those peaks present in the pieces of signal removed.

4.2 Heart and breathing rates detection and their reliability

The proposed algorithm is implemented in the time-domain, thus the heart rate is estimated according to equation (3.7) every 10 seconds while the breathing rate is estimated with equation (3.8) every 60 seconds. Moreover, the reliability of these detected vital signs is computed with the following expressions:

$$K = \frac{|NP - NEP|}{NEP} \tag{4.3}$$

$$\textit{Reliability } [\%] = (1 - K) \cdot 100 \tag{4.4}$$

Where:

- *NP* is the Number of Peaks within the considered window (i.e. 10 seconds for HR and 60 seconds for RR);
- *NEP* is the Number of Expected Peaks with the detected heart or breathing rates.

NEP is computed with the equation (4.5) for the heart rate estimation and with the formula (4.6) for the breathing rate estimation.

$$NEP = \frac{10 \cdot HR}{60} \tag{4.5}$$

$$NEP = \frac{60 \cdot RR}{60} = RR \tag{4.6}$$

Figure 4.10 shows an example of heart and respiratory rates estimates with their respective reliability. It is important to note that the values of the heart and respiratory rates are null, as their reliability, in the pieces of signal affected by noise.

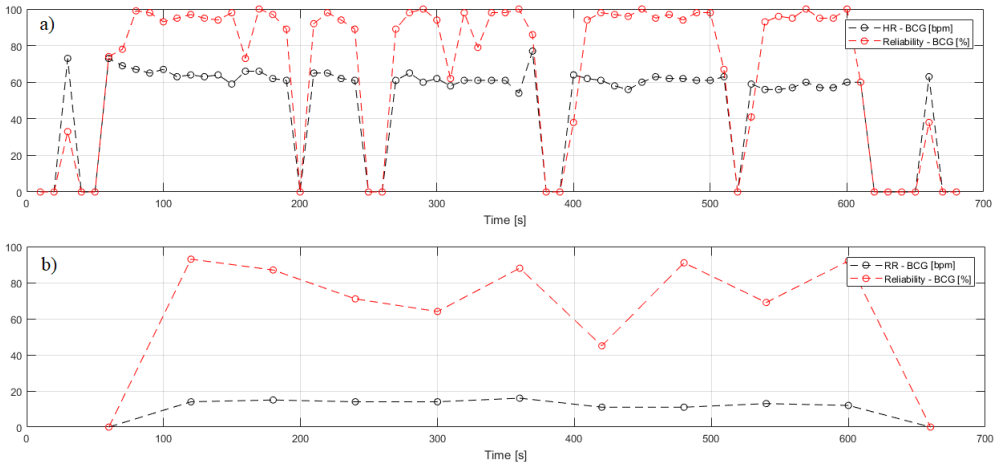

Figure 4.10: Example of detected vital signs; a) detected HR; b) detected RR

Chapter 5

Methodology

A contactless and cost-effective method that could be used to assess cardiorespiratory condition of a subject is the ballistocardiographic technology. In this thesis, a bed-based recording BCG system has been used for nocturnal heart and breathing rates detection. In particular, this chapter describes the details of the employed materials, data set acquisition phase and obtained results. To record the BCG signal, two accelerometric sensors (i.e. the IIS3DHHC and Berkeley accelerometers) were tested, then the one that gave the best results was used for the final application. Finally, in order to validate the extracted heart and breathing rates values, BCG signal recordings have been made simultaneously with the recording of the reference signals (i.e. the ECG and the bioimpedance), acquired through the wearable BodyGateWay (BGW) device.

5.1 Tested accelerometric sensors

The traditional ballistocardiographic technology measures the recoil force of the body and not the body acceleration; consequently, since the used sensors record the accelerometric BCG, this signal can be converted to traditional BCG thanks to the Newton's second law (5.1):

$$F_{body} = m_{body} \cdot a_{body} \tag{5.1}$$

To obtain reliable estimates of heart and breathing rates, a good quality signal must be acquired. For this reason, two sensors (i.e. the IIS3DHHC and the Berkeley accelerometers) have been tested and the one that has provided the best results is used for the final application.

5.1.1 IIS3DHHC accelerometer

The IIS3DHHC is a 3-axis digital accelerometer with ultra-low noise level and excellent stability used as a precision inclinometer[1], in leveling instruments and for antennas and platforms pointing. Its sensing element is produced with a dedicated micromachining process developed by STMicroelectronics to make actuators and inertial sensors on silicon wafers [60].

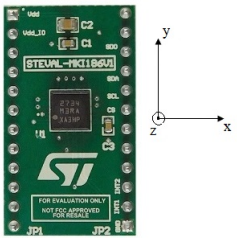

Figure 5.1: The STEVAL-MKI186V1 with IIS3DHHC accelerometer

The main features of this sensor are [60]:

- **Dimensions**: 5x5x1.7 mm;
- **Sensitivity**: 0.076 mg/digit;
- **Full scale**: ± 2.5 g;
- **Noise density**: 45 $\mu g/\sqrt{Hz}$;
- **Supply voltage**: 1.71 - 3.6 V;
- **Supply current**: 2.5 mA;
- **Bandwidth**: 0 - 440 Hz.

[1] An inclinometer is a linear accelerometer with a reduced measuring range generally used to detect slope, or inclination, due to its high sensitivity to variations of the gravitational acceleration

5.1.2 Berkeley accelerometer

The Berkeley accelerometer is generally used in industrial platform heading (tilting application) and in ultra-stable virtual reality. It is installed on a board that includes a STM32-F3 microcontroller, a capacitive digital sensor for humidity and temperature (HTS221) and a digital MEMS accelerometer (Berkeley).

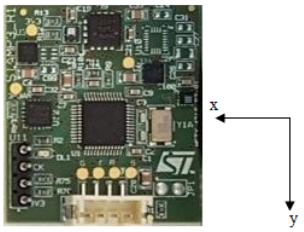

Figure 5.2: The Berkeley board

Specifically, the Berkeley sensor is a low-power and ultra-small dual-axis MEMS inclinometer. Its main characteristics are:

- **Dimensions**: 1.5x5x1.7 mm;
- **Sensitivity**:
  - 0.122 mg/digit with a full scale of ± 4 g;
  - 0.061 mg/digit with a full scale of ± 2 g;
  - 0.0305 mg/digit with a full scale of ± 1 g;
  - 0.01525 mg/digit with a full scale of ± 0.5 g.

  Particularly, to avoid the sensor saturation, only full scale of ± 4 g or ± 2 g can be used because the sensor is placed vertically during the measurements (refer to Section 5.1.3 for details). In order to increase the sensitivity, the full scale is set to ± 2 g.
- **Noise density**: 15 $\mu g/\sqrt{Hz}$;
- **Supply voltage**: 1.71 - 3.6 V;
- **Supply current**: 160 μA in high-performance mode and 3 μA in power-down mode;
- **Bandwidth**: 0 - 52 Hz.

This board is a *plug and play (PnP) device*, i.e. a device that works with a computer system right after its connection [61]. Data is communicated via serial interface, an example of data string is shown below:

X-a [g]	Y-a [g]	T [°C]	RH [%]	Timestamp [10^{-5} s]	Rolling counter [-]
0.026169	0.891149	34.89	52.32	38909557	82836

Where:

- **X-a** is the X-acceleration;
- **Y-a** is the Y-acceleration;
- **T** is the relative temperature;
- **RH** is the relative humidity;
- **Timestamp** is a temporal information that identifies when a certain event occurred;
- **Rolling counter** is a counter that identifies a data string, so it is possible to know if some data has been lost during the acquisition phase. This is a useful information because the *baud rate*, i.e. the rate at which information is transferred in a communication channel [62], is set to 460800 baud. This means that the serial port transfers a maximum of 460800 bits per second (bps).

5.1.3 Comparison between IIS3DHHC and Berkeley

Some preliminary measurements of BCG signal have been performed with IIS3DHHC and Berkeley accelerometers in order to compare the performances of the two sensors based on the noise level contained in the acquired signals. At the beginning, a data acquisition system has been set; subsequently, the output of the two sensors are compared.

Setting of data acquisition system

Each acquisition system needs performing sensors that provide high quality signal. There are sensor positions where the signal is more visible than others, so the sensor should be installed at such location. In particular, the measurements setup is the following:

- **Hardware**: Berkeley or IIS3DHHC accelerometers;
- **Data AcQuisition (DAQ) device**: laptotp and Docklight;
- **No presence of case or fixing tools**: sensor was left below the mattress cover.

Four tests are performed with different position of the sensor on the bed to identify the one that provides the best signal in terms of low noise level.

- **Test 1**: sensor is placed vertically, below the mattress cover, under the pillow and close to the subject head;
- **Test 2**: sensor is placed, vertically, on the mattress lateral wall, below the mattress cover;
- **Test 3**: sensor is placed vertically, below the mattress cover, near to the subject heart;
- **Test 4**: sensor is placed vertically, below the mattress cover, near to the subject feet.

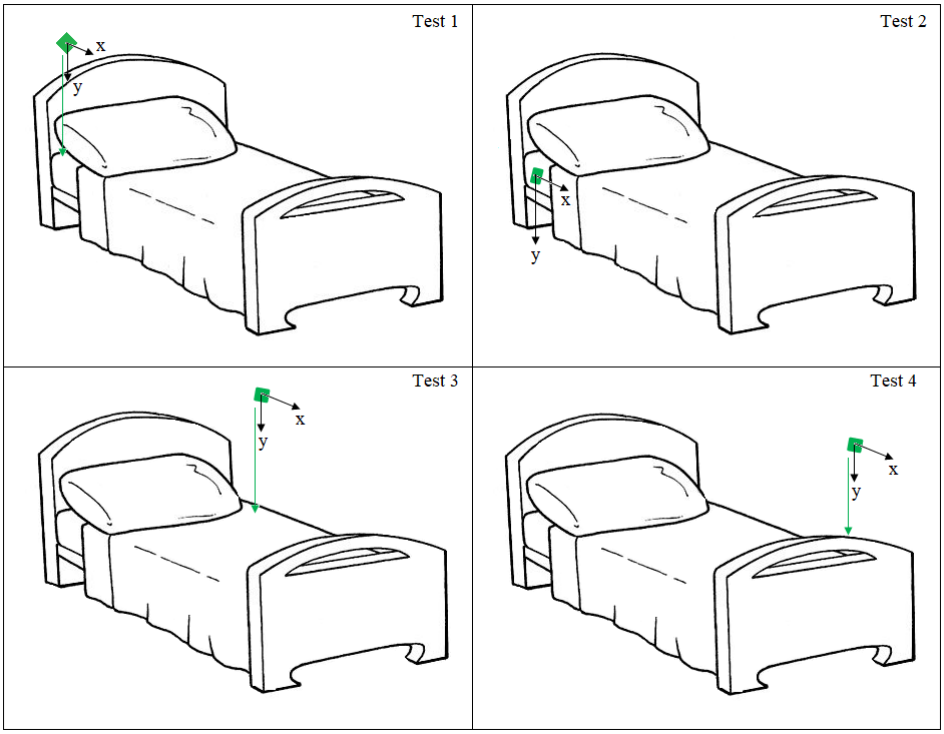

Figure 5.3: Sensor, in green, in the four tested positions

In each configuration shown in Figure 5.3, only the signal component along the x-axis is considered for choosing the sensor position that provides the best signal quality because it represent the longitudinal ballistocardiogram, i.e. the most informative one.

Comparison between the output signal of IIS3DHHC and the output signal of Berkeley

The x-component of the raw signals acquired with the two accelerometers in the four tested positions is shown in Figure 5.4. It is possible to observe that, in each test, the signals acquired with the Berkeley sensor are less affected by noise than those acquired with the IIS3DHHC. In particular, when the sensors are placed near to the subject feet (Test 4), the signal is very clear. Instead, when sensors are placed near to the subject heart (Test 3), the breathing contribution is highly visible; in fact, the sine wave that characterizes the respiratory signal is easily identifiable. Finally, signals obtained in the Test 1 and Test 2 are noisier than those obtained in the Test 4 but still visible.

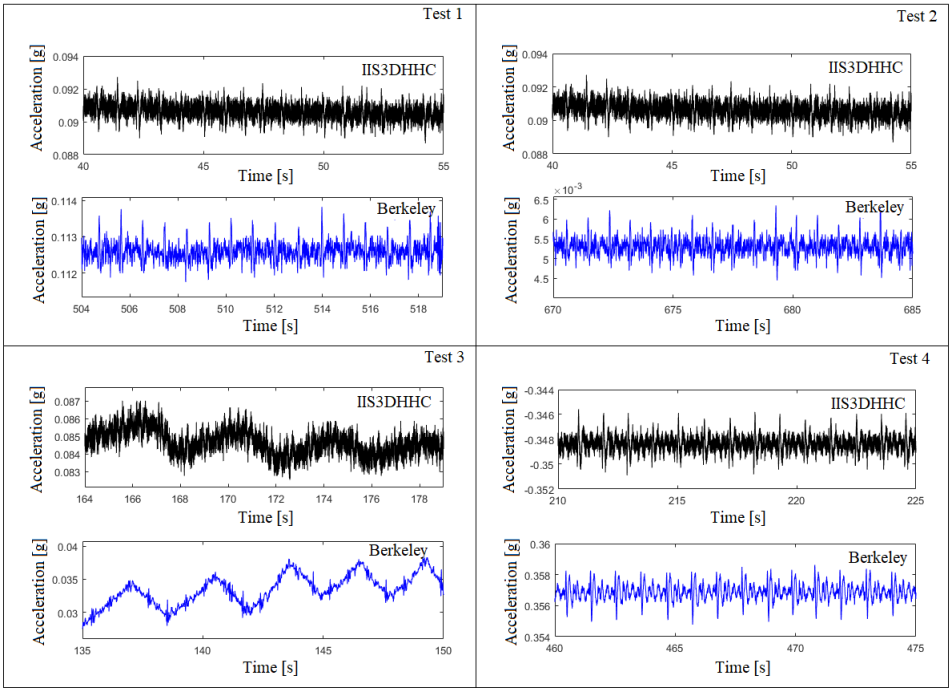

Figure 5.4: Output signals of IIS3DHHC accelerometer and Berkeley in the four tested positions

On the basis of these considerations, since the noise of Berkeley board is remarkably lower than than the IIS3DHHC one, the former sensor has been used for the final application. In addition to the low noise level, its high resolution (given by *noise density*$\cdot\sqrt{bandwidth}$) and small size make the Berkeley inclinometer advantageous for BCG measurement. However, it is possible to distinguish the BCG signal also by using the IIS3DHHC but, in this case, a very careful filtering must be implemented.

5.2 Data set acquisition phase

The performance of the algorithm described in Chapter 4 is evaluated using a data set of 20 recordings from healthy volunteers, including 4 men and 16 women. The main subjects characteristics are summarized in Table 5.1.

Subject	Gender	Age	Height [cm]	Weight [Kg]
1	female	27	170	68
2	female	19	165	58
3	female	47	160	58
4	female	24	162	65
5	male	23	170	64
6	male	28	170	79
7	female	50	167	78
8	female	6	117	20
9	male	48	165	65
10	female	51	165	62
11	female	26	165	70
12	female	18	163	55
13	female	20	170	57
14	female	12	150	47
15	female	48	165	75
16	female	24	158	52
17	female	27	174	66
18	female	77	162	70
19	female	18	165	52
20	male	59	175	76

Table 5.1: Subjects characteristics

The subjects were lying on the bed for approximately 10 - 20 minutes. During this period they were quiet, without any voluntary movement, in order to simulate sleep condition and to minimize motion artifacts. All measurements have been made by placing the sensor as in Test 1 (Figure 5.3). This choice is made to ensure the subject comfort during the measurement; moreover, both the cardiac and respiratory components are clearly visible in this position. Figure 5.5 shows an example raw signal from one subject in the main sleeping postures (i.e.supine, right side, left side and prone). The largest spikes are induced by body movements, such as rolling.

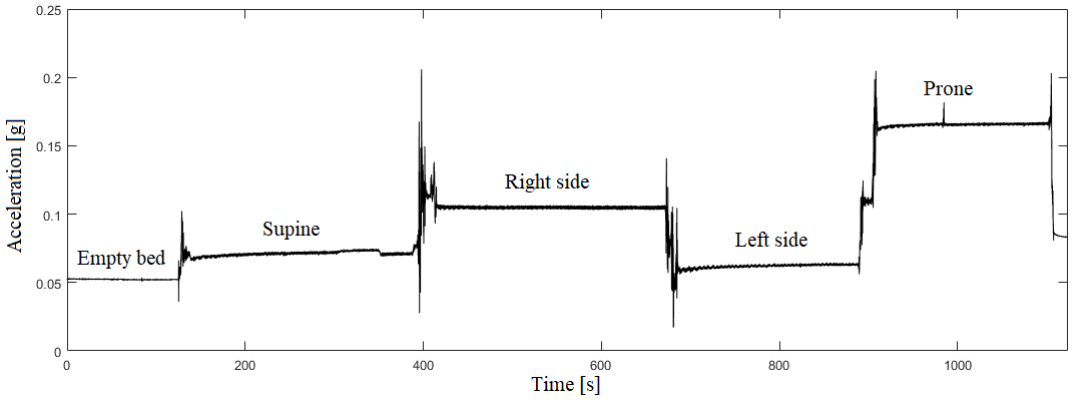

Figure 5.5: Raw acquired data

Figure 5.6 shows the previous example signal after the filtering step; it is possible to observe that there are signal amplitude differences among sleeping postures. Specifically, signal amplitude increases when the subject is in the second sleeping posture because the sensor is placed on the right side of the bed; so sensor and subject are very close. This result is in line with literature; in fact, when the distance between the sensor and subject increases, the amplitude of the signal is lowered [3].

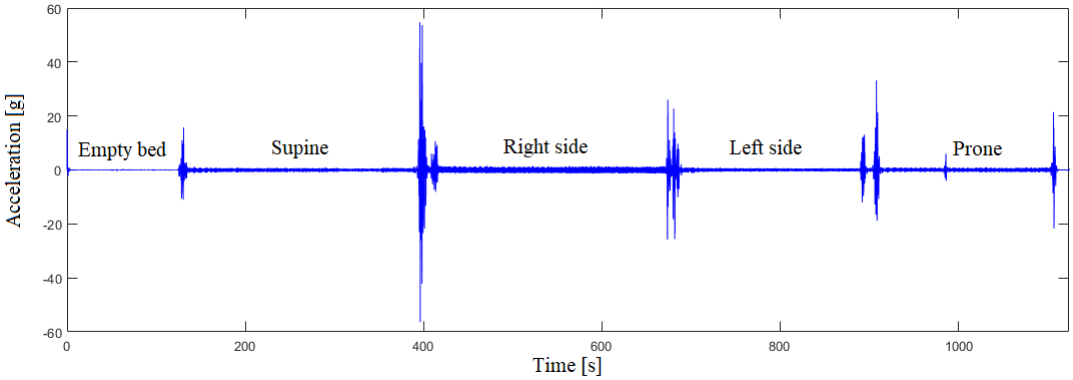

Figure 5.6: Signal Amplitude changes

As mentioned in Section 2.8, the BCG is a 3-D vector. The Berkeley sensor, being a 2-axes accelerometer, records only two BCG components: longitudinal and dorsoventral ballistocardiograms if the board is placed vertically on the bed, longitudinal and transverse ballistocardiograms if the board is placed horizontally on the bed. However, this is not a limit because the most informative content is mainly projected into the longitudinal head-to-foot component. Figure 5.7 shows an example of x and y-components of the filtered

BCG signal; both are modulated by respiration but its contribution is different. For example, the y-component (Figure 5.7 b) is not modulated as much as the x-component (Figure 5.7 a). Moreover, since the x-axis represents the longitudinal direction, the signal amplitude of the x-component is larger than that of the y-component. It is important to note that the signal amplitude does not represent the real amplitude of the BCG signal because the mattress has different spring constants along the x and y axes, thus the signal amplitude is affected by the mechanical properties of the measurement system. Finally, to check the measurement repeatability, tests are made in 5 different beds; in all cases the BCG signal has been successfully recorded.

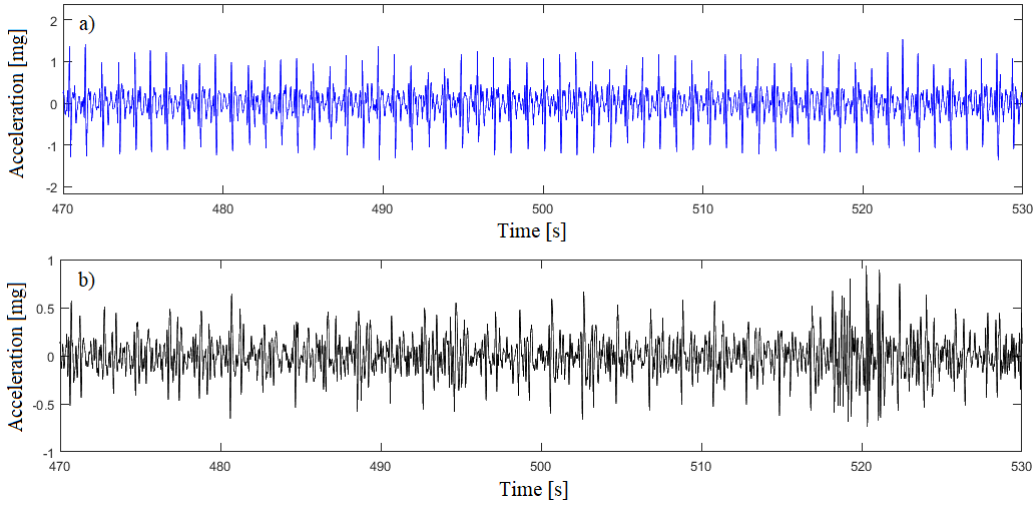

Figure 5.7: Enlarged view of x-component a) and y-component b) of the filtered BCG signal

BCG signal waveforms for all subjects

As mentioned in Section 2.7, the main limitation of the BCG signal, which make it unsuitable for clinical use, is its great inter-subject variability. Figure 5.8 shows some of the acquired signals, from which it is possible to note the differences among the BCG waveforms.

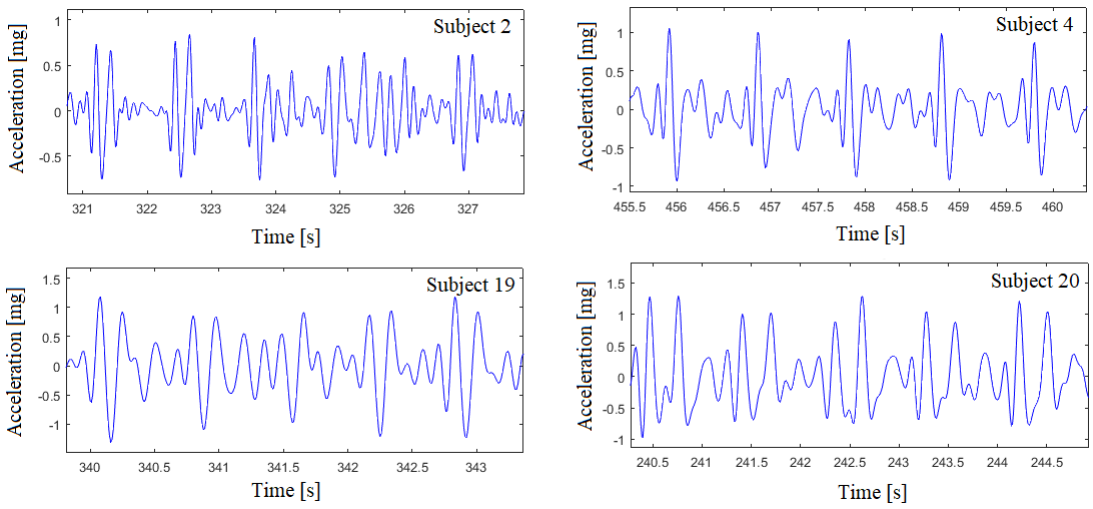

Figure 5.8: Enlarged view of BCG waveforms

5.3 Evaluation of algorithm performance

The detected ballistocardiographic heart and breathing rates have been compared with the heart and breathing rates obtained from the reference device, which is the BodyGateWay, in order to validate the proposed algorithm.

5.3.1 BodyGateWay device

The BodyGateWay is a non-invasive and wearable biomedical device, developed by STMicroelectronics, used for telemedicine purpose. In detail, it is used to monitor heart and breathing rates and to detect physical activity and body posture [63]. The BGW packaging includes a disposable patch and a reusable electronic device. The former is attached to the chest, the latter is connected to the patch. The BGW, after signals acquisition through sensors, processes them. Finally, it transmits the extracted parameters and the recorded raw signals via Bluetooth to a computer, smartphone or tablet. Specifically, digital signal processing and real time elaboration are performed with a low-power microcontroller of the STM32 family.

The BGW with the disposable patch already coupled is shown in the following figure:

Figure 5.9: The BodeGateWay device

In the previous figure 5.9 it is possible to identify 3 LEDs:

- The LED on the left indicates the battery status of charge (the battery is rechargeable);
- The LED on the right provide alerts to the user. When it flashes, it means that the acquired signal is not reliable or the Bluetooth connection is not available;
- The central LED indicates the acquisition mode. If the light is fixed, the device is waiting for external commands (*engaged mode*). When the LED flashes quickly, the device is in *streaming mode*. When the LED flashes slowly, the device is in *monitoring mode*.

Specifically, the BGW device can operate in 4 acquisition modes [63]:

1. **Power down mode**. The BGW is completely turned off;
2. **Engaged mode**. The BGW is visible and connectable to the remote unit via Bluetooth;
3. **Streaming Mode**. The BGW is powered ON and sends data, sampled according to the configuration settings, to the external device with a set periodicity;
4. **Monitoring mode**. The BGW is powered ON. It collects and stores data in the internal memory at the frequency defined in the configuration settings and send this data to the associated device.

The proper body area to which to attach the device in order to acquire reliable signals are shown in Figure 5.10. In particular, the first location is the preferred device placement.

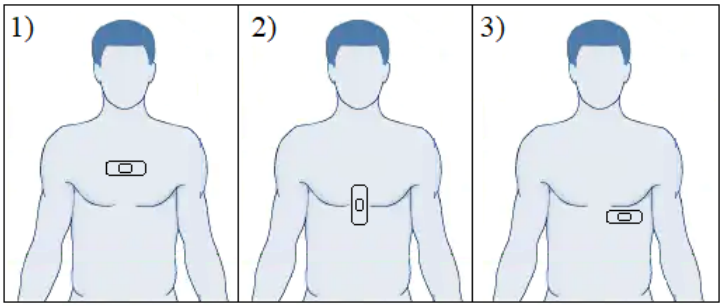

Figure 5.10: Proper area body to which to attach the BGW

The disposable patch includes 4 electrodes (2 electrodes are used to inject an alternating current of 100 μA with a frequency of 50 kHz, the other 2 are used to measure the voltage) with which one lead ECG signal and 2 bioimpedance signals (DC and AC components) are acquired. In particular, the following parameters are extracted from the ECG signal [63]:

- Heart rate;
- RR peak variability;
- Heart Rate variability;
- Electrode detachment alert.

Breathing rate is instead extracted from the bioimpedance signal; body posture and activity level are detected with an accelerometer.

5.4 Results

The algorithm validity has been evaluated by computing statistics indexes. First, for each estimated heart and respiratory rates, the percentage error e_i between the estimate value and the reference value are computed.

$$e_i\ [\%] = \left(\frac{|y_i - x_i|}{y_i} \right) \cdot 100 \tag{5.2}$$

Where:

- i is the i-th measurement;
- y_i is the reference HR or RR value;
- x_i is the estimated HR or RR value.

These errors were then grouped by computing the Mean Absolute Error (MAE), which gives the average magnitude of the errors in a set of estimations.

$$MAE\ [\%] = \frac{1}{N}\sum_{i=1}^{N} e_i \tag{5.3}$$

Where N is the number of errors. The Root Mean Square Error ($RMSE$) and the relative accuracy (ACC) are also computed. The $RMSE$ represents the standard deviation of errors, thus it provides an estimate of how dispersed are the differences between the reference values and measured values. It is an always positive index, with an optimal value equal to zero, typically used in forecasting and regression analysis to validate experimental results.

$$RMSE\ [\%] = \sqrt{\frac{1}{N}\sum_{i=1}^{N} e_i^2} \tag{5.4}$$

$$ACC\ [\%] = \frac{1}{N}\sum_{i=1}^{N} \frac{|y_i - |y_i - x_i||}{y_i} \cdot 100 \tag{5.5}$$

Overall, each R-peak (ECG signal) must be followed by a J-peak (BCG signal); if this condition does not occur, an error is detected. Hence, the *Sensitivity* and the *Positive Predictive Value* (PPV) are calculated. The former, which is the algorithm ability to correctly identify the actual J-peaks (or respiratory peaks), is expressed as:

$$Sensitivity = \frac{TP}{TP + FN} \tag{5.6}$$

Where

- TP is the number of True Positive, which are the J-peaks (or respiratory peaks) correctly identified;
- FN is the number of False Negative, which are the J-peaks (or respiratory peaks) incorrectly rejected;

The PPV is the probability to correctly identify the actual J-peaks (or respiratory peaks). It is expressed as:

$$PPV = \frac{TP}{TP + FP} \tag{5.7}$$

Where FP is the number of False Positive, i.e. the J-peaks (or respiratory peaks) incorrectly identified. The results of the aforementioned statistical indexes relating to the heart rate estimates for each individual recording, with reliability greater than 50%, are shown in the following graphs. Specifically, the discarded signal percentage on acquisitions of an average duration of 14 minutes, is equal to 15.9%. The maximum value obtained (38.3% with a signal duration of 10 minutes) is related to the subject 8 while the minimum value obtained (3.6% with a signal duration of 18 minutes), is related to the subject 4.

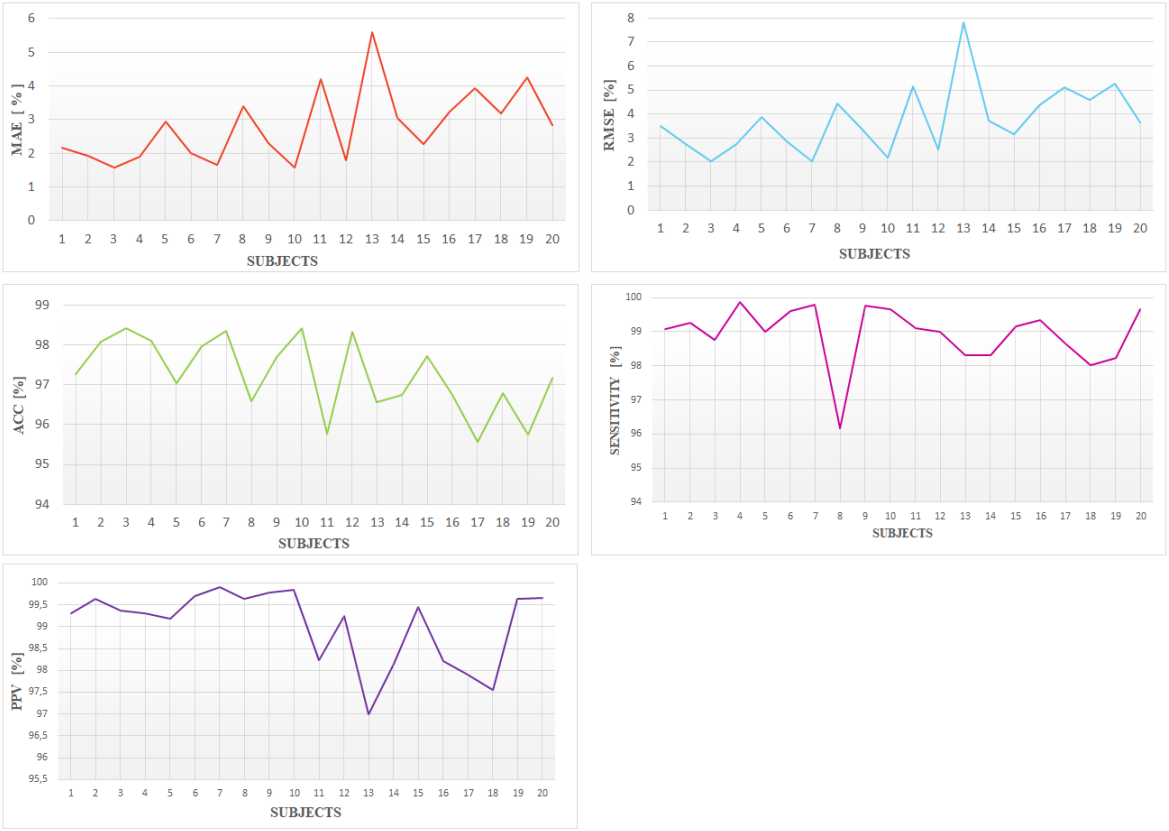

Figure 5.11: Statistical indexes for heart rate estimates

Given the large number of applications developed for cardiac monitoring, the required accuracy varies depending on the application. For example, it has been seen that for measuring the maximal heart rate (HR_{max} = 220 - age), the error should not exceed 3 bpm while it should remain below 8 bpm to detect a training target HR [64]. Consistently, an error of 10% is accepted for clinical use in the case of atrial fibrillation [65]. Most recently, the US national standard of "Heart Rate Monitors, Heart Rate Meters and Alarms" has defined accuracy as:

> "Reading error not exceeding ± 10% of input frequency or ±5 bpm, whichever is greater".

In accordance with these considerations, an acceptable error for heart rate measurements is between 2% and 10%, depending on the application [65]. From the graphs in Figure 5.11, it is possible to observe that the proposed algorithm achieves, on average, a relative accuracy of 97.25% in detecting HR whit an average sensitivity and PPV of 98.94% and 99.04% respectively in identifying J-peaks. The MAE has an average value of 2.79%, thus it is included in the error limits mentioned above. The highest MAE value reached is equal to 5.59%. Finally, the $RMSE$ average value is of 3.76%. To have a clearer view of the errors spread, they have been divided into 4 classes according to the acceptable error limit. Specifically, the error classes are:

- **Error class 1 - EC1**. It includes the errors in the range 0 - 2 %;
- **Error class 2 - EC2**. It includes the errors in the range 3 - 5 %;
- **Error class 3 - EC3**. It includes the errors in the range 6 - 10 %;
- **Error class 4 - EC4**. It includes the errors in the range 11 - 12 %. The upper limit of this class corresponds to the maximum error obtained.

The EC1 elements may be defined as low errors because they are close to the lower limit of acceptable errors; those of EC2 may be defined as medium errors; those of EC3 as high yet still acceptable errors, while EC4 elements are outside the acceptable range. The HR values associated with these last errors are the so-called outliers. These considerations are also valid for the RR error classes, which are reported later. A suitable graph to represent this information is the histogram. It generally shows frequencies of a collection of data, i.e. the number of times an event occurs. However, if data are grouped in class of unequal width, the frequency density replaces the frequency.

$$Frequency\ density = \frac{Frequency}{class\ width} \tag{5.8}$$

In Figure 5.12, each rectangle corresponds to one of the classes mentioned above, as indicated in the key, whose amplitude represents the *class width* while the height corresponds to the *frequency density*. The area of the rectangle is equal to the absolute frequency of the representative class, avoiding thus a distorted representation of the distribution shape.

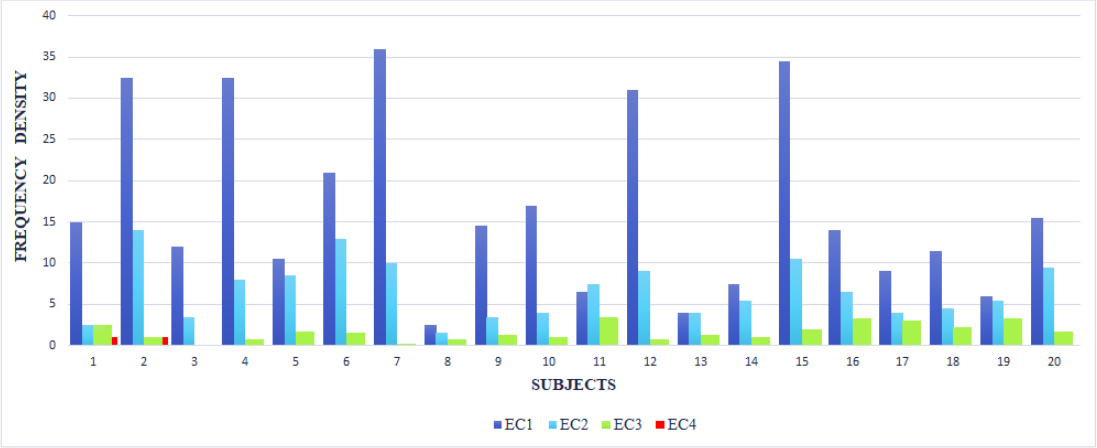

Figure 5.12: Frequency density histogram for HR estimates

In Figure 5.12 it is possible to observe that, for most of the measurements, the percentage error remains within the first and second classes. Furthermore, the outliers are present only 2 times, but in a very low percentage. The same statistical analysis has been done to validate respiratory rate values.

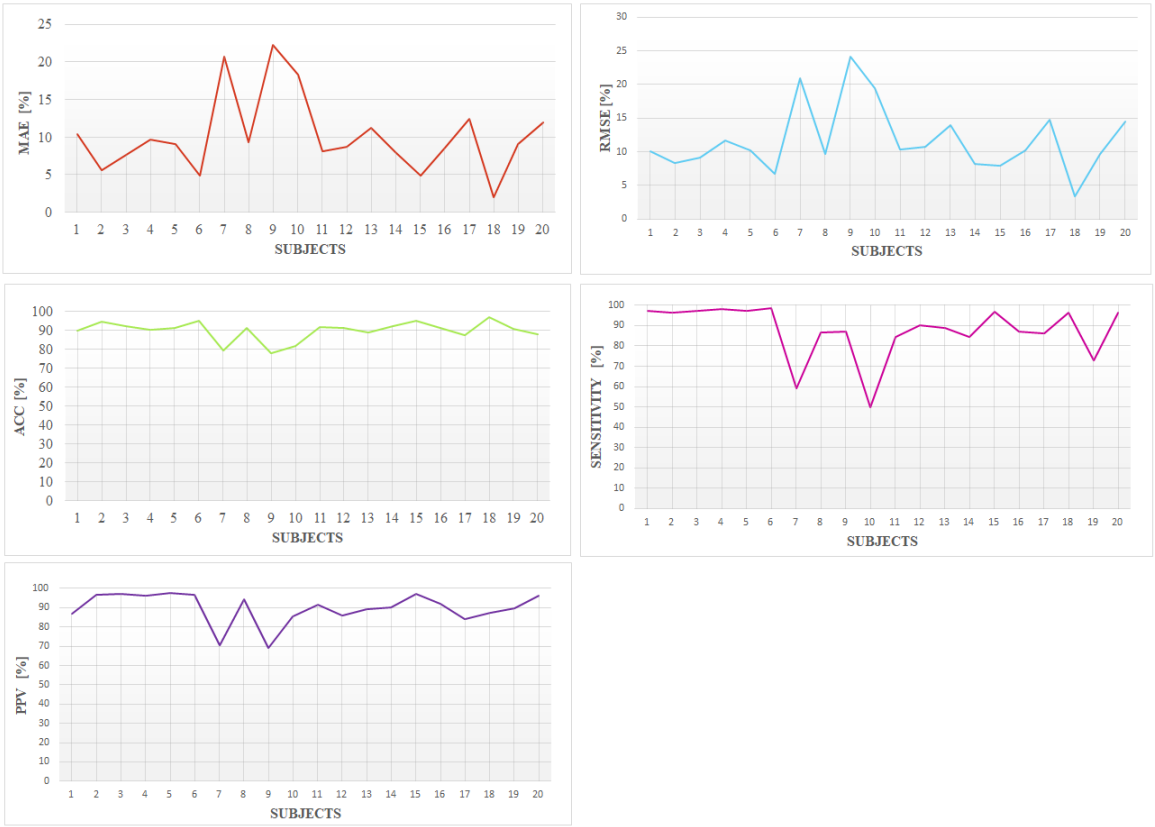

Figure 5.13: Statistical indexes for respiratory rate estimates

From Figure 5.13 it can been seen that, when dealing with respiratory rates, the algorithm performance worsens; in fact, it reaches a relative average accuracy of 89.87% with an average sensitivity of 87.57% and an average PPV of 89.69%. The MAE and the $RMSE$, on average, are of 10.12% and 11.71% respectively. In literature, an accurate measurement of RR is defined as a measure that differs from the reference value of $\pm$ 2 bpm from the reference value [66]. To define the error classes, the RR range of a healthy adult has been considered, ranging from 12 bpm to 20 bpm. The percentage error corresponding to $\pm$ 2 bpm is therefore given by values ranging from 10% to about 17%. The error classes have been divided as follows:

- **Error class 1 - EC1**. It includes errors between 0% and 10%;
- **Error class 2 - EC2**. It includes errors between 11% and 14%;
- **Error class 3 - EC3**. It includes errors between 15% and 17%;

- **Error class 4 - EC4**. It includes errors between 18% and 33%. As for the HR, the upper limit of this class is the maximum error detected in all measurements, equal to an absolute error of 5 bpm.

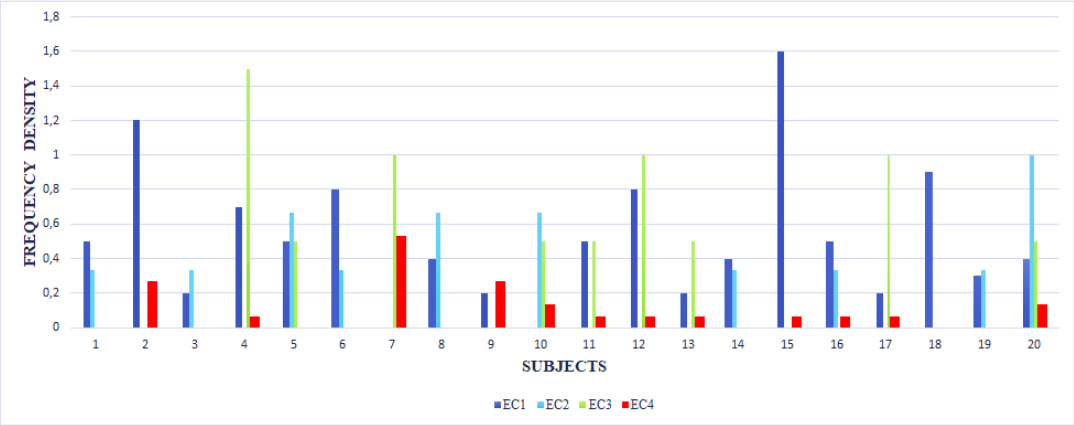

Figure 5.14: Frequency density histogram for RR estimates

Compared to heart rate estimates, the outliers quantity has increased. The error, in most cases, is close to the upper limit of the acceptable range, except for a few cases in which it remains in the first and second class (1st, 3rd, 6th, 8th, 14th, 18th and 19th subjects). Worsening algorithm performance may be associated with the lowest spectral content of the ballistocardiographic respiratory component, and therefore with its difficult extraction.

Chapter 6

Conclusions and future works

This thesis presents a contactless measurement method of heart and respiratory rates from BCG signal, since the need for remote monitoring of cardiorespiratory parameters is growing. The first step is the BCG signal acquisition with an accelerometer properly placed on the bed (the accelerometer is one of the most used sensors in BCG-based applications for the advantages reported in Chapter 3). During this phase, considerations on sensor positioning have been made because it affects the signal quality. After the acquisition system setting, an algorithm has been implemented to extract the vital signs of interest. Subsequently, the algorithm performance has been tested by processing 20 recordings acquired from healthy volunteers. Despite the BCG signal has a small amplitude and it is highly affected by motion artifacts, the results obtained for the heart rate estimates are acceptable and encouraging for the use of this type of application. The results obtained for the breathing rate estimates are less reliable due to the difficult extraction of the ballistocardiographic respiratory component. However, there are still some aspects that need to be investigated, reported below:

1. **Sensitivity of the algorithm to thresholds**;
2. **Outlier management**. Most literature methods replace them with the previous value or with the average of previous values;
3. **Acquisition setup improvement**. This means designing an ad hoc case for the used sensor and a new *Printed Circuit Board* (PCB) dedicated only to this application;
4. **Revision of the thresholds set in the algorithm**. This is a consequence of the previous aspect since the amplitude and morphology of the BCG signal could be influenced by the mechanical properties of the case material and by the lower mass of the new board;

5. **Optimization of the firmware** that manages sensors inside the board and implements the proposed algorithm;

6. **Signal acquisitions over a longer period**, i.e. for the entire night and, possibly, in the hospital environment. In this way, the dataset will be expanded and therefore the validity of the algorithm will be verified;

7. **Sleep quality analysis**. Since the BCG signal can be recorded from a subject lying on the bed, it is particularly suitable for long-term and non-invasive sleep monitoring. In fact, in literature, there are methods that use parameters extracted from the BCG signal (such as HR, HRV, RR, respiratory rate variability, respiratory depth and movements) to detect sleep stages [67], sleep quality and indicators associated with stress.

Bibliography

[1] C. Brüser, C. H. Antink, T. Wartzek, M. Walter, and S. Leonhardt, "Ambient and unobtrusive cardiorespiratory monitoring techniques," *IEEE reviews in biomedical engineering*, vol. 8, pp. 30–43, 2015.

[2] E. Pinheiro, O. Postolache, and P. Girão, "Theory and developments in an unobtrusive cardiovascular system representation: ballistocardiography," *The open biomedical engineering journal*, vol. 4, p. 201, 2010.

[3] X. Feng, Y. Xu, M. Dong, and P. Levy, "Non-contact home health monitoring based on low-cost high-performance accelerometers," in *Proceedings of the Second IEEE/ACM International Conference on Connected Health: Applications, Systems and Engineering Technologies*. IEEE Press, 2017, pp. 356–364.

[4] J. Paalasmaa *et al.*, "Monitoring sleep with force sensor measurement," *Department of Computer Science Series of Publications A*, 2014.

[5] N. V. Thakor and J. G. Webster, "Ground-free ecg recording with two electrodes," *IEEE Transactions on Biomedical Engineering*, no. 12, pp. 699–704, 1980.

[6] D. M. Salerno, "Seismocardiography: A new technique for recording cardiac vibrations. concept, method, and initial observations," *Journal of cardiovascular technology*, vol. 9, no. 2, pp. 111–118, 1990.

[7] C. Barbosa Pereira, M. Czaplik, V. Blazek, S. Leonhardt, and D. Teichmann, "Monitoring of cardiorespiratory signals using thermal imaging: A pilot study on healthy human subjects," *Sensors*, vol. 18, no. 5, p. 1541, 2018.

[8] O. T. Inan, P.-F. Migeotte, K.-S. Park, M. Etemadi, K. Tavakolian, R. Casanella, J. Zanetti, J. Tank, I. Funtova, G. K. Prisk *et al.*, "Ballistocardiography and seismocardiography: A review of recent advances," *IEEE journal of biomedical and health informatics*, vol. 19, no. 4, pp. 1414–1427, 2014.

[9] C. Brüser, S. Winter, and S. Leonhardt, "Robust inter-beat interval estimation in cardiac vibration signals," *Physiological measurement*, vol. 34, no. 2, p. 123, 2013.

[10] A. M. Ferdous, "Scopes and challenges of implementing telemedicine in a developing country like bangladesh," Master's thesis, UiT Norges arktiske universitet, 2017.

[11] A. E. C. P. D. M. L. M. Sara Carrasqueiro, Alfredo Ramalho, "Report on EU state of play on telemedicine services and uptake recommendations," 2017. [Online]. Available: https://ec.europa.eu/health/sites/health/files/ehealth/docs/ev_20171128_co09_en.pdf

[12] D. Friedrich, X. L. Aubert, H. Führ, and A. Brauers, "Heart rate estimation on a beat-to-beat basis via ballistocardiography-a hybrid approach," in *2010 Annual International Conference of the IEEE Engineering in Medicine and Biology*. IEEE, 2010, pp. 4048–4051.

[13] E. J. Pino, C. Larsen, J. Chavez, and P. Aqueveque, "Non-invasive bcg monitoring for non-traditional settings," in *2016 38th annual international conference of the IEEE engineering in medicine and biology society (EMBC)*. IEEE, 2016, pp. 4776–4779.

[14] J. Paalasmaa, H. Toivonen, and M. Partinen, "Adaptive heartbeat modeling for beat-to-beat heart rate measurement in ballistocardiograms," *IEEE journal of biomedical and health informatics*, vol. 19, no. 6, pp. 1945–1952, 2014.

[15] Y.-H. Noh, S.-Y. Ye, and D.-U. Jeong, "Development of the bcg feature extraction methods for unconstrained heart monitoring," in *5th International Conference on Computer Sciences and Convergence Information Technology*. IEEE, 2010, pp. 923–928.

[16] J. Gordon, "Certain molar movements of the human body produced by the circulation of the blood," *Journal of anatomy and physiology*, vol. 11, no. Pt 3, p. 533, 1877.

[17] O. T. Inan, "Recent advances in cardiovascular monitoring using ballistocardiography," in *2012 Annual International Conference of the IEEE Engineering in Medicine and Biology Society*. IEEE, 2012, pp. 5038–5041.

[18] D. Deuchar, "Ballistocardiography." *British heart journal*, vol. 29, no. 3, p. 285, 1967.

[19] R. Soames and J. Atha, "Three-dimensional ballistocardiographic responses to changes of posture," *Clinical Physics and Physiological Measurement*, vol. 3, no. 3, p. 169, 1982.

[20] S. Nurmi *et al.*, "Nocturnal sleep quality and quantity analysis with ballistocardiography," 2016.

[21] R. S. GUBNER, M. RODSTEIN, and H. E. UNGERLEIDER, "Ballistocardiography: An appraisal of technic, physiologic principles, and clinical value," *Circulation*, vol. 7, no. 2, pp. 268–286, 1953.

[22] J. Alametsä, J. Viik, J. Alakare, A. Värri, and A. Palomäki, "Ballistocardiography in sitting and horizontal positions," *Physiological measurement*, vol. 29, no. 9, p. 1071, 2008.

[23] S. Gilaberte, J. Gómez-Clapers, R. Casanella, and R. Pallas-Areny, "Heart and respiratory rate detection on a bathroom scale based on the ballistocardiogram and the continuous wavelet transform," in *2010 Annual International Conference of the IEEE Engineering in Medicine and Biology*. IEEE, 2010, pp. 2557–2560.

[24] A. M. Weissler, "Noninvasive cardiology. grune and stratton," *Inc., New York, NY, USA*, 1974.

[25] W. R. Scarborough, S. A. TALBOT, J. R. BRAUNSTEIN, M. B. RAPPAPORT, W. DOCK, W. R. SCARBOROUGH, W. Hamilton, J. E. SMITH, J. L. NICKERSON, S. A. TALBOT *et al.*, "Proposals for ballistocardiographic nomenclature and conventions: Revised and extended: Report of committee on ballistocardiographic terminology," *Circulation*, vol. 14, no. 3, pp. 435–450, 1956.

[26] Y. Henderson, "The mass-movements of the circulation as shown by a recoil curve," *American Journal of Physiology-Legacy Content*, vol. 14, no. 3, pp. 287–298, 1905.

[27] I. Starr, A. Rawson, H. Schroeder, and N. Joseph, "Studies on the estimation of cardiac ouptut in man, and of abnormalities in cardiac function, from the heart's recoil and the blood's impacts; the ballistocardiogram," *American Journal of Physiology-Legacy Content*, vol. 127, no. 1, pp. 1–28, 1939.

[28] O. Polo, M. Tafti, M. Hamalainen, K. Vaahtoranta, and J. Alihanka, "Respiratory variation of the ballistocardiogram during increased respiratory load and voluntary central apnoea," *European Respiratory Journal*, vol. 5, no. 2, pp. 257–262, 1992.

[29] J. Gomez-Clapers, A. Serra-Rocamora, R. Casanella, and R. Pallas-Areny, "Towards the standardization of ballistocardiography systems for j-peak timing measurement," *Measurement*, vol. 58, pp. 310–316, 2014.

[30] J. Paalasmaa, L. Leppäkorpi, and M. Partinen, "Quantifying respiratory variation with force sensor measurements," in *2011 Annual International Conference of the IEEE Engineering in Medicine and Biology Society*. IEEE, 2011, pp. 3812–3815.

[31] I. Sadek, "Ballistocardiogram signal processing: A literature review," *arXiv preprint arXiv:1807.00951*, 2018.

[32] Y. Hu, E. G. Kim, G. Cao, S. Liu, and Y. Xu, "Physiological acoustic sensing based on accelerometers: A survey for mobile healthcare," *Annals of biomedical engineering*, vol. 42, no. 11, pp. 2264–2277, 2014.

[33] F. Landreani and E. G. Caiani, "Smartphone accelerometers for the detection of heart rate," *Expert review of medical devices*, vol. 14, no. 12, pp. 935–948, 2017.

[34] L. Rosales, B. Y. Su, M. Skubic, and K. Ho, "Heart rate monitoring using hydraulic bed sensor ballistocardiogram 1," *Journal of Ambient Intelligence and Smart Environments*, vol. 9, no. 2, pp. 193–207, 2017.

[35] E. J. Pino, J. A. Chávez, and P. Aqueveque, "Noninvasive ambulatory measurement system of cardiac activity," in *2015 37th annual international conference of the IEEE engineering in medicine and biology society (EMBC)*. IEEE, 2015, pp. 7622–7625.

[36] J. Parak, "Heart rate detection from ballistocardiogram," in *Proceedings of International Student Conference on Electrical Engineering*, vol. 1, 2012, pp. 1–5.

[37] Z. Chen, H. I. Hee, S. H. Ng, J. T. Teo, X. Yang, and D. Wang, "Microbend fiber optic sensor for perioperative pediatric vital signs monitoring," in *Optical Fibers and Sensors for Medical Diagnostics and Treatment Applications XVII*, vol. 10058. International Society for Optics and Photonics, 2017, p. 100580L.

[38] S. Poeggel, D. Tosi, D. Duraibabu, G. Leen, D. McGrath, and E. Lewis, "Optical fibre pressure sensors in medical applications," *Sensors*, vol. 15, no. 7, pp. 17 115–17 148, 2015.

[39] C. Brüser, A. Kerekes, S. Winter, and S. Leonhardt, "Multi-channel optical sensor-array for measuring ballistocardiograms and respiratory activity in bed," in *2012 Annual International Conference of the IEEE Engineering in Medicine and Biology Society*. IEEE, 2012, pp. 5042–5045.

[40] M. Brink, C. H. Müller, and C. Schierz, "Contact-free measurement of heart rate, respiration rate, and body movements during sleep," *Behavior research methods*, vol. 38, no. 3, pp. 511–521, 2006.

[41] J. Paalasmaa, "A respiratory latent variable model for mechanically measured heartbeats," *Physiological measurement*, vol. 31, no. 10, p. 1331, 2010.

[42] A. Albukhari, F. Lima, and U. Mescheder, "Bed-embedded heart and respiration rates detection by longitudinal ballistocardiography and pattern recognition," *Sensors*, vol. 19, no. 6, p. 1451, 2019.

[43] J. Paalasmaa and M. Ranta, "Detecting heartbeats in the ballistocardiogram with clustering," in *Proceedings of the ICML/UAI/COLT 2008 workshop on machine learning for health-care applications, Helsinki, Finland*, vol. 9, 2008.

[44] J. Shin, B. Choi, Y. Lim, D. Jeong, and K. Park, "Automatic ballistocardiogram (bcg) beat detection using a template matching approach," in *2008 30th Annual International Conference of the IEEE Engineering in Medicine and Biology Society*. IEEE, 2008, pp. 1144–1146.

[45] A. Akhbardeh, S. Junnila, M. Koivuluoma, T. Koivistoinen, and A. Varri, "Evaluation of heart condition based on ballistocardiogram classification using compactly supported wavelet transforms and neural networks," in *Proceedings of 2005 IEEE Conference on Control Applications, 2005. CCA 2005.* IEEE, 2005, pp. 843–848.

[46] A. Akhbardeh, M. Koivuluoma, T. Koivistainen, and A. Varri, "Bcg data clustering using new method so-called time-frequency moments singular value decomposition (tfm-svd) and artificial neural networks," in *Proceedings of the 2005 IEEE International Symposium on, Mediterrean Conference on Control and Automation Intelligent Control, 2005.* IEEE, 2005, pp. 1447–1451.

[47] X. Yu, D. Gong, X. Shuen, S. Li, and Y. Xu, "Comparisons of a combined wavelet and a combined principal component analysis classification model for bcg signal analysis," in *IEEE International Conference on Robotics, Intelligent Systems and Signal Processing, 2003. Proceedings. 2003*, vol. 1. IEEE, 2003, pp. 160–165.

[48] S. Karki and J. Lekkala, "Film-type transducer materials pvdf and emfi in the measurement of heart and respiration rates," in *2008 30th annual international conference of the IEEE engineering in medicine and biology society.* IEEE, 2008, pp. 530–533.

[49] J. M. Kortelainen and J. Virkkala, "Fft averaging of multichannel bcg signals from bed mattress sensor to improve estimation of heart beat interval," in *2007 29th annual international conference of the IEEE engineering in medicine and biology society*. IEEE, 2007, pp. 6685–6688.

[50] M. Obaidat, "Phonocardiogram signal analysis: techniques and performance comparison," *Journal of Medical Engineering & Technology*, vol. 17, no. 6, pp. 221–227, 1993.

[51] A. Moukadem, A. Finnaoui, H. E. Gassara, D. Adolphe, L. Schacher, and A. Dieterlen, "Time-frequency domain for bcg analysis," in *2018 International Conference on Computer and Applications (ICCA)*. IEEE, 2018, pp. 226–230.

[52] A. Taebi and H. Mansy, "Time-frequency distribution of seismocardiographic signals: A comparative study," *Bioengineering*, vol. 4, no. 2, p. 32, 2017.

[53] O. B. Fosso and M. Molinas, "Method for mode mixing separation in empirical mode decomposition," *arXiv preprint arXiv:1709.05547*, 2017.

[54] Z. Wu and N. E. Huang, "Ensemble empirical mode decomposition: a noise-assisted data analysis method," *Advances in adaptive data analysis*, vol. 1, no. 01, pp. 1–41, 2009.

[55] M. Xiao, C. Zhang, K. Wen, L. Xiong, G. Geng, and D. Wu, "Bearing fault feature extraction method based on complete ensemble empirical mode decomposition with adaptive noise." *Journal of Vibroengineering*, vol. 20, no. 7, 2018.

[56] F. Wang, M. Tanaka, and S. Chonan, "Development of a pvdf piezopolymer sensor for unconstrained in-sleep cardiorespiratory monitoring," *Journal of intelligent material systems and structures*, vol. 14, no. 3, pp. 185–190, 2003.

[57] X. Zhu, W. Chen, T. Nemoto, Y. Kanemitsu, K.-i. Kitamura, K.-i. Yamakoshi, and D. Wei, "Real-time monitoring of respiration rhythm and pulse rate during sleep," *IEEE transactions on biomedical engineering*, vol. 53, no. 12, pp. 2553–2563, 2006.

[58] S.-T. Choe and W.-D. Cho, "Simplified real-time heartbeat detection in ballistocardiography using a dispersion-maximum method," 2017.

[59] B. Kohler, C. Hennig, and R. Orglmeister, "Qrs detection using zero crossing counts," *Applied genomics and proteomics*, vol. 2, no. 2, pp. 138–145, 2003.

[60] STMicroelectronics, *IIS3DHHC Datasheet*, 2018. [Online]. Available: https://www.st.com/resource/en/datasheet/iis3dhhc.pdf

[61] Plug and play definition. [Online]. Available: https://techterms.com/definition/plugandplay

[62] What is baud rate why is it important? [Online]. Available: https://www.setra.com/blog/what-is-baud-rate-and-what-cable-length-is-required-1

[63] St microelectronics s.r.l. bodyguardian control unit body gateway. [Online]. Available: https://usermanual.wiki/ST-Microelectronics-S-R-L/MHBGW1.Product-literature

[64] R. A. Robergs and R. Landwehr, "The surprising history of the" hrmax= 220-age" equation," *Journal of Exercise Physiology Online*, vol. 5, no. 2, pp. 1–10, 2002.

[65] F. Sartor, J. Gelissen, R. Van Dinther, D. Roovers, G. B. Papini, and G. Coppola, "Wrist-worn optical and chest strap heart rate comparison in a heterogeneous sample of healthy individuals and in coronary artery disease patients," *BMC Sports Science, Medicine and Rehabilitation*, vol. 10, no. 1, p. 10, 2018.

[66] N. Keshvani, K. Berger, O. K. Nguyen, and A. N. Makam, "Roadmap for improving the accuracy of respiratory rate measurements," *BMJ Qual Saf*, vol. 27, no. 8, pp. e5–e5, 2018.

[67] S. Nurmi, T. Saaresranta, T. Koivisto, U. Meriheinä, L. Palva *et al.*, "Validation of an accelerometer based bcg method for sleep analysis," 2016.